EXPERIMENTAL AND THEORETICAL STUDIES OF LIQUID SLOSHING AT SIMULATED LOW GRAVITIES

by

Franklin T. Dodge
Luis R. Garza

20 October 1966

N67 13111

FACILITY FORM 602

(ACCESSION NUMBER)   78   (THRU)

(PAGES)

CR-80471   (CODE)

(NASA CR OR TMX OR AD NUMBER)   (CATEGORY)

SOUTHWEST RESEARCH INSTITUTE
SAN ANTONIO   HOUSTON

SOUTHWEST RESEARCH INSTITUTE
8500 Culebra Road, San Antonio, Texas 78206

Department of Mechanical Sciences

EXPERIMENTAL AND THEORETICAL STUDIES OF LIQUID SLOSHING AT SIMULATED LOW GRAVITIES

by

Franklin T. Dodge
Luis R. Garza

20 October 1966

APPROVED:

H. Norman Abramson, Director
Department of Mechanical
Sciences

ABSTRACT

_13 111_

      An analysis is given for liquid sloshing in a rigid cylindrical tank under conditions of moderately low gravitational acceleration; the theory is valid for Bond numbers that are larger than 10. The results are put in the form of an equivalent mechanical model. It is found that both the fundamental sloshing mass and the natural frequency, for a liquid having a zero degree contact angle, are smaller than for the usual high-g sloshing.

      A series of experiments was conducted to determine the sloshing force and the natural frequency for Bond numbers between 10 and 200. The test results are compared to the theoretical predictions of the mechanical model, and good correlation between theory and experiment is shown.

Author

TABLE OF CONTENTS

LIST OF ILLUSTRATIONS

LIST OF ILLUSTRATIONS (Cont'd)

LIST OF PRINCIPAL SYMBOLS*

A_n — amplitude of the time variation of the nth component of the velocity potential

$a_n = A_n \cos \Omega \tau$

B_n — amplitude of the time variation of the nth component of the surface wave

$b_n = B_n \sin \Omega \tau$

$C1_{nm}$,
$C2_{nm}$, — Fourier-Bessel coefficients in Eqs. (21) and (22)
$C3_{nm}$

F — lateral force exerted on the tank by the liquid

F_T — interfacial tension force at contact line

$f(F)$ — height of meniscus above $z = 0$, see Figure 1

g — steady axial acceleration or gravity

H_n — dimensionless wave height of nth mode at the wall

h_{av} — average depth of liquid, $m_T / \pi \rho R_o^2$

$h_{c.m.}$ — height of center-of-mass above tank bottom

h_n — height of m_n above tank bottom

h_o — height of m_o above tank bottom

$$I_n = \sum_{m=1}^{M} P_{nm} J_1(\lambda_m) e^{\lambda_m \beta} / \lambda_m, \text{ see Eq. (34)}$$

J_1 — 1st order Bessel function of the first kind

k_n — spring constant for n^{th} mode

$$L_n = \sum_{m=1}^{M} (h/R_o - \beta - 1/\lambda_m) P_{nm} J_1(\lambda_m) e^{\lambda_m \beta} / \lambda_m, \text{ see Eq. (43)}$$

*Symbols in parenthesis are the nondimensional equivalents of the preceding quantities.

M	-	number of terms in potential equation or number of slosh masses
m_n	-	sloshing mass of nth mode
m_o	-	mass rigidly attached to tank
m_T	-	total liquid mass
N_{BO}	-	Bond number, $\rho g R_o^2/T$
P_{mn}	-	amplitude of that part of a_n associated with the natural frequency Ω_m
p	-	liquid pressure
p_g	-	ullage gas pressure
p_o	-	liquid pressure at $r = 0$, $z = 0$
Q_{nm}	-	amplitude of that part of b_n associated with the natural frequency Ω_m
R_o	-	radius of tank
$r(R)$ θ $z(Z)$	-	axes of cylindrical coordinate system, see Figure 1
T	-	interfacial tension
$t(\tau)$	-	time
$x_o(X_o)$	-	excitation amplitude
β	-	nondimensional meniscus height at tank wall
ζ	-	total wave height above $z = 0$, see Figure 1
$\eta(\epsilon)$	-	wave height above meniscus, see Figure 1
θ_c	-	contact angle of liquid on tank wall, measured in the liquid
λ_n	-	roots of $J_1'(\lambda_n) = 0$
ρ	-	density of liquid
$\phi(\Phi)$	-	velocity potential
Ω_n	-	dimensionless natural frequency of nth mode
$\omega(\Omega)$	-	frequency

I. INTRODUCTION

The free surface wave motions ("sloshing") of liquid fuel in large rocket boosters is a well-recognized problem in technology. While nearly all the experimental and theoretical work on the practical side of this problem is limited to situations in which the steady axial acceleration (gravity or thrust or both) is so large that only the body forces in the liquid and the forces between the tank walls and the liquid need be considered for determining the liquid's motion, there are occasions when the axial acceleration is small, as for example when the booster is coasting in an Earth orbit, and then other forces must be taken into account; the most important of these forces is usually the interfacial tension between the liquid fuel and the ullage gas. Under these conditions, the resulting free surface motion has been called low-gravity sloshing.

Most of the previous research on low-gravity fluid mechanics is reviewed in Ref. [1], which also contains a lengthy list of references. The reports by Reynolds and his coworkers [2, 3] are especially recommended. More recent developments are given in Refs. [4] and [5]. To the authors' knowledge, however, there are no experimental or theoretical results available for the important problem of the sloshing of the liquid during forced excitation of the tank (although the generalized analysis given in Ref. [4] can supposedly be specialized to include this).

In this report, an analysis and experimental correlations of low-gravity sloshing in a cylindrical tank are presented for the case of simple harmonic translation of the rigid tank. Now, experimental data for low-gravity sloshing

are not easily obtained. Ground facilities that can duplicate an actual low-gravitational acceleration, such as drop towers, are not able to provide the low-gravity field for a sufficiently long time to get consistent and reliable sloshing data because the testing time available is on the order of only five seconds; drop towers, though, are quite valuable for experiments on other aspects of low-gravity fluid mechanics. Another method of simulating low gravity is to use small models in a bench test; the interfacial or capillary forces can be made comparable to, or greater than, the gravity forces even in the one-g field, so this is a suitable "low-gravity" test for some purposes. The available test time is not a problem with this kind of simulation, but the liquid motion and the slosh forces are, of course, quite small because of the small dimensions of the model. In the experiments reported here, the low-gravity simulation was accomplished by this method of using small models; such a simulation required that an extremely sensitive dynamometer system be designed and constructed (slosh forces smaller than 0.001 pound were expected). The resulting data, to the authors' knowledge, are the first (and the only up to now) that present sloshing forces and frequencies as a function of Bond number; these are the parameters that are of most value in missile and space applications. (Some data for natural frequencies have been published previously [3].)

The axial acceleration and the tank dimensions used in the tests were small enough that the Bond number, $N_{BO} = \rho g R_o^2 / T$, an indication of the size of body forces relative to interfacial forces, was in the range of 10 to 100.

Very low-gravity fluid mechanics are characterized by Bond numbers of less than one, while high-g problems are in the range of $N_{BO} > 1000$. Thus, $10 \leq N_{BO} \leq 100$ should be classified as moderately low gravities*. Even though body forces are still dominant for these Bond numbers (but not over-whelmingly so) interfacial tension causes the undisturbed equilibrium free surface to depart considerably from a flat surface, and, thus, interfacial curvature and forces must be included in the analysis.

Effects such as stratification and thermally driven motions are ignored in the analysis and are absent in the experimental tests. Moreover, the influence of viscosity is neglected in the analysis since experience has shown it to be small; the main effects can be accounted for a posteriori by adding suitable linear damping. The circular cylindrical tank is assumed to be rigid.

The theoretical analysis is given first; the experimental procedure and test results follow, and the correlations between theory and experiment are then presented.

---

*Bond numbers of this size, for example, are encountered in coasting orbits of large boost stages such as Saturn IVB [6].

II. ANALYSIS

A.   Basic Equations

An r, θ , z cylindrical coordinate system is <u>fixed</u> in the tank and centered along the axis at the point the axis intersects the undisturbed free surface, as shown in Figure 1.* The depth of liquid below z = 0 is taken to be large enough that the tank bottom is essentially at z = - ∞ ; this assumption greatly simplifies the algebraic work and is valid if $h/2R_o > 1$. The height, f(r), of the undisturbed axisymmetric free surface is measured positively above z = 0; the wave height, $\eta(r, \theta, t)$, is then measured from the undisturbed surface and not from z = 0.

By assuming that the ideal liquid is incompressible and its motion irrotational, a velocity potential, $\phi(r, \theta, z, t)$, may be defined such that the liquid velocity relative to the tank is $\vec{V} = \nabla\phi$. The potential must satisfy Laplace's equation

$$\nabla^2\phi = \frac{1}{r}\frac{\partial}{\partial r}\left(r\,\frac{\partial\phi}{\partial r}\right) + \frac{1}{r^2}\frac{\partial^2\phi}{\partial\theta^2} + \frac{\partial^2\phi}{\partial z^2} = 0 \tag{1}$$

and two conditions at the tank boundaries

$$\frac{\partial\phi}{\partial r} = 0 \quad , \quad r = R_o \tag{2}$$

$$\frac{\partial\phi}{\partial z} = 0 \quad , \quad z = -\infty \tag{3}$$

If the velocities and density of the ullage gas are neglected, the first integral of the equations of motion evaluated just below the free surface gives

---

*All figures grouped in Appendix B.

one relation for determining the wave height from the velocity potential; it is

$$\frac{\partial \phi}{\partial t} + \frac{p}{\rho} + \frac{1}{2}[\nabla \phi \cdot \nabla \phi] + g\zeta - x_o \omega^2 r \cos \theta \cos \omega t = \psi(t) \quad , \quad z = \zeta \qquad (4)$$

$\zeta(r, \theta, t) = \eta(r, \theta, t) + f(r)$ is the wave height above $z = 0$, and $\psi(t)$ is a function of time at most.

A second condition between ζ and ϕ is obtained by requiring that the normal stress across the free surface must be discontinuous by an amount proportional to the product of the interfacial tension, T, and the mean surface curvature:

$$P_g - p = T \left(\frac{1}{r} \frac{\partial}{\partial r} \left\{ \frac{r \frac{\partial \zeta}{\partial r}}{\left[1 + \left(\frac{\partial \zeta}{\partial r} \right)^2 + \left(\frac{1}{r} \frac{\partial \zeta}{\partial \theta} \right)^2 \right]^{1/2}} \right\} \right.$$
$$\left. + \frac{1}{r^2} \frac{\partial}{\partial \theta} \left\{ \frac{\frac{\partial \zeta}{\partial \theta}}{\left[1 + \left(\frac{\partial \zeta}{\partial r} \right)^2 + \left(\frac{1}{r} \frac{\partial \zeta}{\partial \theta} \right)^2 \right]^{1/2}} \right\} \right) \quad , \quad z = \zeta \qquad (5)$$

A final condition between ζ and ϕ arises from the fact that the motion of the free surface and the fluid velocity at the free surface must be consistent with each other, or

$$\frac{\partial \zeta}{\partial t} - \frac{\partial \phi}{\partial z} + \frac{\partial \phi}{\partial r} \left(\frac{\partial \zeta}{\partial r} \right) + \frac{1}{r^2} \left(\frac{\partial \phi}{\partial \theta} \right) \left(\frac{\partial \zeta}{\partial \theta} \right) = 0 \quad , \quad z = \zeta \qquad (6)$$

The final requirement for a well-posed problem is knowledge of the angle at which the free surface meets the tank walls. * Here it is assumed that the contact angle measured in the liquid, for the undisturbed surface, is zero, which is typical of several existing fuel-tank systems; any other angle could be used in the analysis just as easily. It is entirely possible that the angle at which the sloshing wave meets the walls differs from the undisturbed angle; this phenonemon is known as "contact angle hysteresis." Some researchers have tried to account for the hysteresis by assuming that

$$\frac{\partial \eta}{\partial r} = C_1 \eta \quad , \quad z = \zeta \quad r = R_0$$

which seems to imply that the change in the contact angle depends only on the distance the free surface is displaced from equilibrium. (C_1 is an experimentally determined constant.) But the hysteresis, should also be a strong function of the contact line velocity because, in a sufficiently slow movement, the contact angle should stay reasonably close to its static value. Thus, rather than assume an arbitrary functional relationship, hysteresis is neglected in the analysis, and the contact line is allowed to slide easily along the tank walls — the so-called "free edge" condition. Hence, the contact line condition used here is

$$\frac{\partial \eta}{\partial r} = 0 \quad , \quad z = \zeta \quad r = R_0. \tag{7}$$

Actually, the contact angle is defined by $\theta_c = \cot^{-1} \left\{ \frac{\partial \zeta}{\partial r} \middle/ \left[1 + \left(\frac{\partial \zeta}{r \partial \theta} \right)^2 \right]^{1/2} \right\}$

(at $r = R_0$) so that Eq. (7) allows θ_c to vary from its static value, which is

---

*In high-g analyses, the free surface is flat at equilibrium and is assumed to deform to whatever shape the dynamics require, regardless of the value of the contact angle.

$\cot^{-1}$ (df/dr). However, since $\partial\zeta/\partial r = df/dr + \partial\eta/\partial r$, if the equations are linearized with respect to η (which will be done presently), then Eq. (7) says that θ_c always equals its static value.

B. Equilibrium Interface

The equilibrium free surface shape, f(r), must be known as an input to the sloshing analysis. It can be computed as part of the analysis, say, in the form of a series of the eigenfunctions of Eq. (1) [4], but this process does not converge very quickly; or it can be obtained from a numerical solution of the equations, but this virtually forces the entire sloshing analysis to be numerical. Fortunately, very good approximate algebraic expressions can be derived for f(r) in the range of Bond numbers of interest here.

In Eq. (4) let $\phi \equiv 0$, and in Eq. (5) let $\psi(t) = p_0/\rho$, where p_0 is the liquid pressure at r = 0, z = 0. Now, the pressure at any other point on the free surface in the liquid is

$$p = p_0 - \rho g f(r) \tag{4'}$$

and the interface tension-curvature relation is

$$p = p_g - T\left(\frac{1}{r}\frac{d}{dr}\left\{\frac{r\frac{df}{dr}}{\left[1+\left(\frac{df}{dr}\right)^2\right]^{1/2}}\right\}\right) \tag{5'}$$

where p_g is the ullage gas pressure. Thus, combining Eqs. (4') and (5'), it is found that

$$\left(\frac{1}{r}\frac{d}{dr}\left\{\frac{r\frac{df}{dr}}{\left[1+\left(\frac{df}{dr}\right)^2\right]^{1/2}}\right\}\right)_{r=0} - \frac{1}{r}\frac{d}{dr}\left\{\frac{r\frac{df}{dr}}{\left[1+\left(\frac{df}{dr}\right)^2\right]^{1/2}}\right\} + \frac{\rho g}{T}f = 0 \tag{8}$$

This equation with the boundary conditions $f = df/dr = 0$ at $r = 0$ and $df/dr = \cot \theta_c = \infty$ at $r = R_o$ completely determines $f(r)$.

At very small Bond numbers, the equilibrium interface is nearly spherical [i.e., $f(r) = R_o - (R_o^2 - r^2)^{1/2}$]. As the Bond number increases, the interface becomes flatter. Using this as a guide, Satterlee and Chin [7] showed that a modified spherical shape, $f(r) = \beta[R_o - (R_o^2 - r^2)^{1/2}]$ with β a function of N_{BO}, was an approximate solution of Eq. (8) which agreed well with experiments and exact solutions if $N_{BO} < 10$; for larger Bond numbers, the assumed shape, however, was not "flat" enough. Thus, for a range of N_{BO} greater than 10, a reasonable assumption for $f(r)$ is

$$f(r) = \beta R_o \left[1 - \left(1 - \frac{r^3}{R_o^3} \right)^{1/2} \right] \tag{9}$$

since the curvature of this is considerably less than that of a sphere except very close to the walls. β is calculated such a way that Eq. (8) is approximately satisfied in some sense. Now, Eq. (9) already satisfies the proper boundary conditions, and Eq. (8) at $r = 0$; if β is picked so that Eq. (8) is also satisfied at $r = R_o$, then Eq. (9) should give a reasonable prediction of $f(r)$. Carrying out the details yields the result that

$$\beta^3 N_{BO} - \beta^2 - \frac{2}{3} = 0 \tag{10}$$

Eqs. (9) and (10) compare very well with Satterlee and Chin's experimental data for $N_{BO} > 10$ [7].

C.   Linearized Sloshing Equations

The potential, ϕ, and the wave height, η, are now assumed to be small enough that the equations may be linearized with respect to them; note

that neither $f(r)$ nor $\zeta(r, \theta, t)$ need be small, though. After combining Eqs. (4) and (5) and subtracting out the equilibrium condition, Eq. (8), the linearized pressure requirement at the free surface is found to be

$$\frac{\partial \phi}{\partial t} + g\eta - \frac{T}{\rho}\left(\frac{1}{r}\frac{\partial}{\partial r}\left\{ \frac{r\frac{\partial \eta}{\partial r}}{\left[1 + \left(\frac{df}{dr}\right)^2\right]^{3/2}} \right\} + \frac{1}{r^2}\frac{\partial}{\partial \theta}\left\{ \frac{\frac{\partial \eta}{\partial \theta}}{\left[1 + \left(\frac{df}{dr}\right)^2\right]^{1/2}} \right\} \right)$$

$$= x_0 \omega^2 r \cos \theta \sin \omega t = 0 \quad z = f(r) \qquad (11)$$

and now this equation is evaluated on the undisturbed interface, $z = f(r)$. Linearizing Eq. (6), the kinematic condition, gives

$$\frac{\partial \eta}{\partial t} - \frac{\partial \phi}{\partial z} + \frac{df}{dr}\left(\frac{\partial \phi}{\partial r}\right) = 0 \quad , \quad z = f(r) \qquad (12)$$

This completes the linearization of the basic equations.

The entire set of equations are nondimensionalized by using the following substitutions:

$$R = r/R_o \quad ; \quad Z = z/R_o \quad ; \quad \tau = t(g/R_o)^{1/2} \quad ; \quad N_{BO} = \rho g R_o^2/T \quad ;$$

$$F = f/R_o \quad ; \quad \epsilon = \eta/R_o \quad ; \quad \Phi = \phi(gR_o^3)^{-1/2} \quad ; \quad X_o = x_o/R_o$$

$$\Omega = \omega(R_o/g)^{1/2}*$$

For convenience, the nondimensional equations are listed below:

$$\nabla^2 \Phi = 0 \quad \text{in the liquid} \qquad (13)$$

---

*For very small Bond numbers, a better nondimensionalization of ω is $\overline{\Omega} = \omega(\rho R_o^3/T) = \Omega N_{BO}$ since this avoids any difficulties in the dimensionless frequency as $g \to 0$.

$$\frac{\partial \Phi}{\partial R} = 0 \quad , \quad R = 1 \tag{14}$$

$$\frac{\partial \Phi}{\partial Z} = 0 \quad , \quad Z = -\infty \tag{15}$$

$$\frac{\partial \epsilon}{\partial R} = 0 \quad , \quad R = 1 \quad Z = F(1) = \beta \tag{16}$$

$$\frac{\partial \epsilon}{\partial \tau} - \frac{\partial \Phi}{\partial Z} + \frac{dF}{dR}\left(\frac{\partial \Phi}{\partial R}\right) = 0 \quad , \quad Z = F \tag{17}$$

$$\frac{\partial \Phi}{\partial \tau} + \epsilon - \frac{1}{N_{BO}}\left(\frac{1}{R}\frac{\partial}{\partial R}\left\{\frac{R\frac{\partial \epsilon}{\partial R}}{\left[1 + \left(\frac{dF}{dR}\right)^2\right]^{3/2}}\right\} + \frac{1}{R^2}\frac{\partial}{\partial \theta}\left\{\frac{\frac{\partial \epsilon}{\partial \theta}}{\left[1 + \left(\frac{dF}{dR}\right)^2\right]^{1/2}}\right\}\right)$$

$$- X_o \Omega^2 R \cos \theta \sin \Omega t = 0 \quad , \quad Z = F \tag{18}$$

and $F(R) = \beta[1 - (1 - R^3)^{1/2}]$ with β determined by $\beta^3 N_{BO} - \beta^2 - 2/3 = 0$.

D.   Solution

Unfortunately, no function or set of functions known to the authors will exactly satisfy the field equation, Eq. (13), and all the boundary conditions, Eqs. (14) through (18). Of several approximate methods, the one selected here is to construct a solution from the known set of solutions for sloshing at very large Bond numbers for which $F = 0$. This seems reasonable because body forces are still the largest forces when $N_{BO} > 10$. Thus, a velocity potential of the following form is assumed to be acceptable:

$$\Phi(R, \theta, Z, \tau) = \sum_{n=1}^{\infty} a_n(\tau) \cdot J_1(\lambda_n R) \cdot \cos \theta \cdot e^{\lambda_n Z} \tag{19}$$

If the λ_n are determined from $J_1'(\lambda_n) = 0$, Eq. (19) identically satisfies term by term Eqs. (13), (14), and (15).* This will also insure that each $J_1(\lambda_n R)$ is orthogonal to all the rest in the interval $0 \leq R \leq 1$, with the weighting function R.

Boundary condition, Eq. (16), is satisfied if

$$\epsilon(R, \theta, \tau) = \sum_{n=1}^{\infty} b_n(\tau) \cdot J_1(\lambda_n R) \cdot \cos \theta \tag{20}$$

This type of expansion for ϵ cannot be made to satisfy a contact line condition of the form $\partial \epsilon / \partial R = C_1 \epsilon$, and consequently only the free edge condition $(C_1 = 0)$ can be analyzed with Eq. (20).

Now, if $F \equiv 0$ (i.e., if $N_{BO} = \infty$) Eqs. (17) and (18) reduce to

$$\dot{b}_n - \lambda_n a_n = 0 \tag{17'}$$

$$\dot{a}_n + b_n - \frac{2X_o \Omega^2}{(\lambda_n^2 - 1) J_1(\lambda_n)} \sin \Omega \tau = 0 \tag{18'}$$

These equations result from dividing through by $J_1(\lambda_n) \cos \theta$ in each of the orthogonal equations. Thus, a_n and b_n can be easily determined, and the potential and the wave shape are completely defined.** Using Eqs. (17') and (18') as a guide, every term in Eqs. (17) and (18) is expanded in a Bessel-Fourier series of the form:

---

*$\lambda_1 = 1.84118$, $\lambda_2 = 5.33144$, $\lambda_3 = 8.53632$, $\lambda_4 = 11.70600, \ldots$,
$\lambda_{n+1} \approx \lambda_n + \pi$ [8].

**It turns out that $a_n = \dfrac{-2X_o \Omega^3}{(\lambda_n^2 - 1) J_1(\lambda_n)(\Omega^2 - \lambda_n)} \cos \Omega \tau$ and, in particular,

$a_1 = -\dfrac{1.438 X_o \Omega^3}{\Omega^2 - 1.841} \cos \Omega \tau.$

$$\sum_{m=1}^{\infty} C_m J_1(\lambda_m R) \cos \theta$$

Now, Eq. (17) reduces to

$$\sum_{n=1}^{\infty} \left\{ \dot{b}_n + \sum_{m=1}^{\infty} C1_{nm} a_m \right\} J_1(\lambda_n R) \cos \theta = 0 \tag{21}$$

and Eq. (18) reduces to

$$\sum_{n=1}^{\infty} \left\{ b_n + \sum_{m=1}^{\infty} C2_{nm} \dot{a}_m + \sum_{m=1}^{\infty} C3_{nm} b_m \right.$$

$$\left. - \frac{2X_o \Omega^2}{(\lambda_n^2 - 1) J_1(\lambda_n)} \sin \Omega \tau \right\} J_1(\lambda_n R) \cos \theta = 0 \tag{22}$$

where $C1_{nm}$, $C2_{nm}$, and $C3_{nm}$ are the functions of β and N_{BO} given in Appendix A. Since the $J_1(\lambda_n R)$ are orthogonal, each term in the sums over n in Eqs. (21) and (22) must be identically zero. Hence, after combining Eqs. (21) and (22) to eliminate the $b_n(\tau)$, the equation for each $a_n(\tau)$ is found to be

$$\sum_{m=1}^{\infty} C2_{nm} \ddot{a}_m - \sum_{m=1}^{\infty} C1_{nm} a_m - \sum_{s=1}^{\infty} \left(C3_{ns} \sum_{m=1}^{\infty} C1_{sm} a_m \right)$$

$$= \frac{2X_o \Omega^3}{(\lambda_n^2 - 1) J_1(\lambda_n)} \cos \Omega \tau = 0 \tag{23}$$

It follows that each a_n depends on all the rest. Adequate results, however, can be obtained for the first few modes by truncating the equations at, say, m = M, and then treating the resulting set of equations by ordinary methods.

Each of the set of M equations in M unknowns can then be put into a form such as

$$\ddot{a}_n + \xi_{n1}a_n + \sum_{\substack{m=1 \\ m \neq n}}^{M} (\xi_{m2}\ddot{a}_m + \xi_{m3}a_m) = X_o\Omega^3\xi_{n4}\cos\Omega\tau \quad , \quad n = 1, 2, \ldots, M$$

(24)

where the ξ_{ij} are numerical constants. For example, with $N_{BO} = 20$ ($\beta = 0.340$) and $m = 3$, the equations to be solved are

$$\ddot{a}_1 + 1.750a_1 + (-0.375\ddot{a}_2 + 1.138a_2) + (0.608\ddot{a}_3 - 2.093a_3)$$

$$= 1.147X_o\Omega^3 \cos \Omega\tau$$

$$(-0.129\ddot{a}_1 - 0.365a_1) + \ddot{a}_2 + 9.304a_2 + (-0.666\ddot{a}_3 - 1.427a_3)$$

$$= -0.130X_o\Omega^3 \cos \Omega\tau$$

$$(0.065\ddot{a}_1 + 0.503a_1) + (-0.260\ddot{a}_2 - 4.589a_2) + \ddot{a}_3 + 28.229a_3$$

$$= 0.042X_o\Omega^3 \cos \Omega\tau$$

The b_n's are calculated from Eq. (21), which for this case is

$$\dot{b}_3 = 0.345a_1 - 3.213a_2 + 17.083a_3$$

$$\dot{b}_1 = 2.071a_1 - 0.456a_2 + 1.554a_3$$

$$\dot{b}_2 = -0.373a_1 + 7.445a_2 - 3.993a_3$$

Only the steady state response of Eqs. (24) is desired, so letting $a_n = A_n \cos \Omega\tau$, substituting this expression into Eqs. (24), and then solving for the A_n shows that the A_n are of the following general form:

$$A_n = \left[\frac{K_{1n}\Omega^{2n} + K_{2n}\Omega^{2n-2} + \ldots + K_{Mn}\Omega^2}{\Omega^{2n} + K_1\Omega^{2n-2} + \ldots + K_{M-1}\Omega^2 + K_M}\right]X_o\Omega$$

(25)

K_{ij} and K_i are various products of the constants in Eqs. (24). This equation can be put into a more revealing form by rearranging it according to the ideas of partial fractions:

$$A_n = \left[\frac{P_{1n}}{\Omega^2 - \Omega_1^2} + \frac{P_{2n}}{\Omega^2 - \Omega_2^2} + \ldots + \frac{P_{Mn}}{\Omega^2 - \Omega_M^2} \right] X_o \Omega^3 \qquad (26)$$

The Ω_i^2, which are the factors of the denominator in Eq. (25), can be identified as the square of the natural frequency of the ith sloshing mode; they are ordered such that $\Omega_1^2 < \Omega_2^2 < \ldots < \Omega_M^2$. Physical reasoning implies that all the $\Omega_i^2 > 0$, and this turns out always to be the case.

By substituting these results into Eq. (19) and rearranging the terms according to natural frequency, the velocity potential may be expressed as

$$\Phi = X_o \Omega^3 \cos\theta \cos\Omega\tau \sum_{n=1}^{M} \frac{1}{\Omega^2 - \Omega_n^2} \left\{ \sum_{m=1}^{M} P_{nm} J_1(\lambda_m R) e^{\lambda_m Z} \right\} \qquad (27)$$

The sum in braces in Eq. (27) is the normal mode function for the nth sloshing mode (not normalized to one). Note that the index n in P_{nm} in Eq. (27) occupies the first position in the subscript, while, in Eq. (26), it occupies the second; thus, all the A_n contribute to each mode of Φ.

Now, by letting $b_n = B_n \sin\Omega\tau$, Eq. (21) shows that

$$B_n = \left[\frac{Q_{1n}}{\Omega^2 - \Omega_1^2} + \frac{Q_{2n}}{\Omega^2 - \Omega_2^2} + \ldots + \frac{Q_{Mn}}{\Omega^2 - \Omega_M^2} \right] X_o \Omega^2 \qquad (28)$$

in which the Q_{ij} are various products of the constants in Eq. (21) and the P_{ij}. Thus, the dimensionless wave shape is:

$$\epsilon = X_o \Omega^2 \cos \theta \sin \Omega\tau \sum_{n=1}^{M} \frac{1}{\Omega^2 - \Omega_n^2} \left\{ \sum_{m=1}^{M} Q_{nm} J_1(\lambda_m) \right\} \qquad (29)$$

The velocity potential, Φ, and the wave shape, ϵ, have now been determined. The appropriate terms can be easily picked out of Φ and ϵ for studying any particular mode; as will be seen, this is of considerable help in formulating an equivalent mechanical model.

As a numerical example, let $N_{BO} = 20$, $\beta = 0.340$, and $M = 3$ as before. Then, using the previous results, the A_n are

$$A_1 = \left[-\frac{1.158}{\Omega^2 - 1.819} - \frac{0.002}{\Omega^2 - 10.373} - \frac{0.007}{\Omega^2 - 31.797} \right] X_o \Omega^3$$

$$A_2 = \left[-\frac{0.027}{\Omega^2 - 1.819} - \frac{0.016}{\Omega^2 - 10.373} + \frac{0.012}{\Omega^2 - 31.797} \right] X_o \Omega^3$$

$$A_3 = \left[\frac{0.001}{\Omega^2 - 1.819} + \frac{0.015}{\Omega^2 - 10.373} + \frac{0.020}{\Omega^2 - 31.797} \right] X_o \Omega^3$$

(A_3 is not determined quite so accurately as A_2, which in turn is probably less accurately determined than A_1. In general, one would expect that the A_n for n near M will not be as accurately calculated as for smaller n; i.e., if another $M' > M$ is picked, then the previously calculated A_n for n near M will be changed somewhat. This is not an important limitation because only the first mode results are needed in most applications.) For the numerical example, the B_n are

$$B_1 = \left[-\frac{2.384}{\Omega^2 - 1.819} + \frac{0.023}{\Omega^2 - 10.373} + \frac{0.012}{\Omega^2 - 31.797} \right] X_o \Omega^2$$

$$B_2 = \left[\frac{0.227}{\Omega^2 - 1.814} - \frac{0.170}{\Omega^2 - 10.373} + \frac{0.012}{\Omega^2 - 31.797} \right] X_0 \Omega^2$$

$$B_3 = \left[-\frac{0.295}{\Omega^2 - 1.819} + \frac{0.272}{\Omega^2 - 10.373} + \frac{0.336}{\Omega^2 - 31.797} \right] X_0 \Omega^2$$

Thus, the fundamental sloshing mode for $N_{BO} = 20$ is

$$\frac{X_0 \Omega^3 \cos \Omega \tau \cos \theta}{\Omega^2 - 1.819} [-1.158 J_1(1.841R) e^{1.841Z} - 0.027 J_1(5.331R) e^{5.331Z}$$

$$+ 0.001 J_1(8.536R) e^{8.536Z}]$$

and the fundamental wave shape is

$$\frac{X_0 \Omega^2 \sin \Omega \tau \cos \theta}{\Omega^2 - 1.819} [-2.384 J_1(1.841R) + 0.227 J_1(5.331R) - 0.295 J_1(8.536R)]$$

For comparison purposes, the first three dimensionless sloshing frequencies when $N_{BO} = \infty$ are $(1.841)^{1/2}$, $(5.331)^{1/2}$, and $(8.536)^{1/2}$. When $N_{BO} = 20$ but $\theta_c = \pi/2$, i.e., no surface curvature, the frequencies are $(2.?)^{1/2}$, $(12.906)^{1/2}$, and $(39.634)^{1/2}$ [9]*. According to the present analysis, the frequencies for $N_{BO} = 20$ and $\theta_c = 0$ are $(1.819)^{1/2}$, $(10.373)^{1/2}$, and $(31.797)^{1/2}$. Thus, the conclusion is that interfacial tension "stiffens" the free surface but that surface curvature, which depends greatly on the contact angle, "relaxes" it.

The dimensionless natural frequency parameter $\Omega_1^2 = \omega_1^2 R_0/g$ for the first mode is shown as a function of the Bond number in Figure 2. Ω_1^2 for $10 \le N_{BO} \le 100$ is always less than the high-g limit, $\Omega_1^2 = 1.841$, and approaches this value rather slowly as $N_{BO} \rightarrow \infty$. The frequency equation of Ref. [3],

---

*The set of Eqs. (13) through (18) can be solved exactly for this case since F = 0 and the boundary conditions "separate" term by term.

$\Omega_1^2 = 1.841 + (6.26 - 4.76 \cos\theta_c)/N_{BO} = 1.841 + 1.50/N_{BO}$ for $\theta_c = 0$, is also

shown for comparison purposes; as will be seen, however, the results of the

present theory give the best comparison with the trend of Ω^2 vs N_{BO} from

our experiments; in any case, the difference between the present theory, the

theory of Ref. [3] and the high-g theory is always less than about 5 percent

for $10 \leq N_{BO} \leq 100$.

E.   Equivalent Mechanical Model

The sloshing characteristics important in missile applications are

primarily the slosh frequencies and the forces and moments exerted on the

tank. These characteristics are displayed in a more convenient from for

stability and control analyses by an equivalent (mathematical) mechanical

model. Moreover, the results of the partially numerical analysis must be

presented in graphical form, which is a form especially suited for a set of

lumped parameters such as springs and masses. Finally, damping can be

introduced in a straightforward manner in the mechanical model.

The proposed model, shown in Figure 3, is outwardly similar to

other slosh models; as can be seen, one spring-mass oscillator is included

for each of the M slosh modes. In order to calculate the parameters m_o,

$m_1, \ldots, k_1, k_2, \ldots, h_o, h_1, \ldots$, the forces and moments exerted on the

tank by the liquid must be known.

The interfacial tension forces acting on the tank walls along an element

ds of the contact line is shown in the sketch at the top of page 18; these forces

arise as a consequence of considering the interfacial tension to be similar to

a stretched membrane. The force in the plane of the wall, $F_T = T \cos\theta_c \, ds$,

acts as shown; since here θ_c is always 0, thus $F_T = TR_o \, d\theta$ because $ds = R_o \, d\theta$
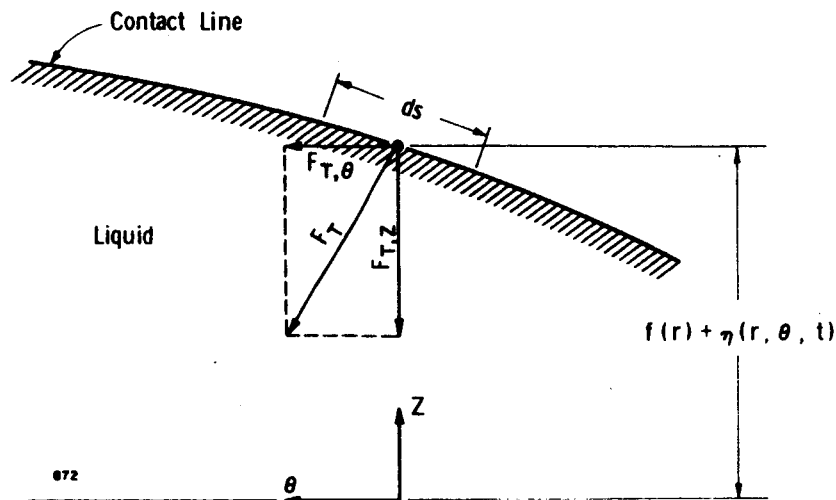
when higher order products of η are neglected. The vertical component of F_T is also F_T, to the first order in η, and the component of F_T tangential to the tank walls in the increasing θ direction is $F_{T,\theta} = F_T \dfrac{\partial \eta}{\partial \theta}$. Thus, the net force on the tank is composed of a vertical force, which is not important here, and the vector sum of the $F_{T,\theta} \cdot ds$ forces, which turns out only to

be a resultant in the direction of the tank excitation. The net horizontal force, then, caused directly by interfacial tension is

$$F_1 = - \int_0^{2\pi} \frac{\partial \eta (r = R_o)}{\partial \theta} T \sin \theta \, d\theta$$

Since $\eta = R_o \epsilon$, after the integration this equation becomes

$$F_1 = \pi X_o \Omega^2 T R_o \sin \Omega \tau \sum_{n=1}^{M} \frac{H_n}{\Omega^2 - \Omega_n^2} \tag{30}$$

where $H_n = \displaystyle\sum_{m=1}^{M} Q_{nm} J_1(\lambda_m)$ is the dimensionless wave height at the wall for the nth mode. Now, $T = \rho g R_o^2 / N_{BO}$ so Eq. (30) reduces to:

$$F_1 = \left(\frac{1}{N_{BO}}\right)\pi\rho R_o^3 x_o \omega^2 \sin \omega t \sum_{n=1}^{M} \frac{H_n \frac{g}{R_o}}{\omega^2 - \Omega_n^2 \frac{g}{R_o}} \tag{31}$$

after resubstituting dimensional variables back in.

The part of the force directly attributable to the liquid's motion can be calculated with the aid of the velocity potential. Since Φ can be used only in an accelerating reference frame moving with the tank, a velocity potential for particles moving with the tank must be added to Φ before forces in an inertial frame can be computed. Thus, let $\Psi = \Phi + X_o \Omega R \cos \theta \times \cos \Omega \tau$. Then, if products of Ψ with itself are neglected, the liquid pressure is

$$p = -\rho g R_o \left(\frac{\partial \Psi}{\partial \tau} + Z\right)$$

or

$$p = -\rho g R_o \left(\frac{\partial \Phi}{\partial \tau} - X_o \Omega^2 R \cos \theta \sin \Omega \tau + Z\right)$$

In this equation p, has its usual dimensions but is expressed in terms of the dimensionless coordinates R, θ, Z, τ. Thus, the force is

$$F_2 = R_o^2 \int_0^{2\pi} \int_{-\frac{h}{R_o}}^{\frac{\zeta_o}{R_o}} [p(R=1)] \cos \theta \, dZ \, d\theta$$

where $\zeta_o = \zeta(r = R_o) = R_o F(1) + R_o \epsilon(R = 1) = \beta R_o + R_o \epsilon_o$. Hence

$$F_2 = -\rho g R_o^3 \int_0^{2\pi} \int_{-\frac{h}{R_o}}^{\beta + \epsilon_o} \left[\frac{\partial \Phi(R=1)}{\partial \tau} - X_o \Omega^2 \cos \theta \sin \Omega \tau + Z\right] \cos \theta \, dZ \, d\theta$$

The last term in the integral is

$$\int_0^{2\pi} \int_{-\frac{h}{R_o}}^{\beta + \epsilon_o} Z \cos\theta \, dZ \, d\theta = \frac{1}{2} \int_0^{2\pi} \left[\beta^2 + 2\beta\epsilon_o + \epsilon_o^2 - \left(\frac{h}{R_o}\right)^2\right] \cos\theta \, d\theta$$

The first and last terms in Eq. (32) integrate to zero; the next-to-last term is a second order quantity in ϵ and is negligible;* Eq. (32) thus reduces to

$$\int_0^{2\pi} \int_{-\frac{h}{R_o}}^{\beta + \epsilon_o} Z \cos\theta \, dZ \, d\theta = \beta \int_0^{2\pi} \epsilon_o \cos\theta \, d\theta$$

$$= \pi\beta X_o \Omega^2 \sin\Omega\tau \sum_{m=1}^{M} \frac{H_n}{\Omega^2 - \Omega_n^2} \tag{33}$$

Similarly, since products of Φ and ϵ are negligible, the first term in the force integral is

$$\int_0^{2\pi} \int_{-\frac{h}{R_o}}^{\beta + \epsilon_o} \frac{\partial\Phi}{\partial\tau} \cos\theta \, dZ \, d\theta = -\pi X_o \Omega^4 \sin\Omega\tau \sum_{n=1}^{M} \frac{I_n}{\Omega^2 - \Omega_n^2} \tag{34}$$

where $I_n = \sum_{m=1}^{M} \frac{P_{nm}}{\lambda_m} J_1(\lambda_m) e^{\lambda_m \beta}$, and it already has been assumed that h/R_o is so large that $e^{-\lambda_m h/R_o} \approx 0$. The results then show that

$$F_2 = \pi\rho R_o^3 x_o \omega^2 \sin\omega t \left\{ \beta + \frac{h}{R_o} - \beta \sum_{n=1}^{M} \frac{H_n \frac{g}{R_o}}{\omega^2 - \Omega_n^2 \frac{g}{R_o}} + \omega^2 \sum_{n=1}^{M} \frac{I_n}{\omega^2 - \Omega_n^2 \frac{g}{R_o}} \right\}$$

$$\tag{35}$$

---

*The entire integral is negligible for very large Bond numbers.

and the total force, $F_1 + F_2$, acting on the tank walls is

$$F = \pi \rho R_o^3 x_o \omega^2 \sin \omega t \left\{ \beta + \frac{h}{R_o} - \left(\beta - \frac{1}{N_{BO}} \right) \sum_{n=1}^{M} \frac{H_n \frac{g}{R_o}}{\omega^2 - \Omega_n^2 \frac{g}{R_o}} \right.$$

$$\left. + \omega^2 \sum_{n=1}^{M} \frac{I_n}{\omega^2 - \Omega_n^2 \frac{g}{R_o}} \right\}$$

After combining and rearranging various terms, it can be seen that

$$F = \pi \rho R_o^3 x_o \omega^2 \sin \omega t \left\{ \frac{h}{R_o} + \left[\beta + \left(\beta - \frac{1}{N_{BO}} \right) \sum_{n=1}^{M} \frac{H_n}{\Omega_n^2} \right] \right.$$

$$\left. + \omega^2 \sum_{n=1}^{M} \frac{I_n - \left(\beta - \frac{1}{N_{BO}} \right) \frac{H_n}{\Omega_n^2}}{\omega^2 - \Omega_n^2 \frac{g}{R_o}} \right\} \qquad (36)$$

Now, by calculating the late~~ral forces on the tank walls due to the system~~ of masses and springs in the mechanical model, one finds that

$$F_{model} = x_o \omega^2 \sin \omega t \left[m_o + \sum_{n=1}^{M} m_n - \omega^2 \sum_{n=1}^{M} \frac{m_n}{\omega^2 - \frac{K_n}{m_n}} \right] \qquad (37)$$

The mechanical model will give forces equivalent to the sloshing, then, if

$$m_n = - \left[I_n - \left(\beta - \frac{1}{N_{BO}} \right) \frac{H_n}{\Omega_n^2} \right] \qquad (38)$$

$$\frac{K_n}{m_n} = \Omega_n^2 \frac{g}{R_o} \qquad (39)$$

and

$$m_o + \sum_{n=1}^{M} m_n = \pi\rho R_o^3 \left[\frac{h}{R_o} + \beta + \left(\beta - \frac{1}{N_{BO}} \right) \sum_{n=1}^{M} \frac{H_n}{\Omega_n^2} \right] \tag{40}$$

The numerical calculations show that $\pi\rho R_o^3 \left[\frac{h}{R_o} + \beta + \left(\beta - \frac{1}{N_{BO}} \right) \sum_{n=1}^{M} \frac{H_n}{\Omega_n^2} \right]$

is always very nearly equal to the total mass of the liquid, which is

$m_T = \rho\pi R_o^3 (h/R_o + 0.264\beta)$; as $M \rightarrow \infty$, it is reasonable to believe that it

would equal the liquid mass exactly, although this would probably be difficult

to prove in complete generality. Assuming, then, that the term is equal to

m_T, Eq. (40) shows that

$$m_o + \sum_{n=1}^{M} m_n = m_T \tag{40'}$$

It would be surprising if the part of the force directly proportional to the

acceleration of the tank were not equal to the product of the liquid mass and

the acceleration. Note that both m_n and k_n can be computed from knowledge

of only the nth sloshing mode and surface wave; in other words, m_n and k_n

are not coupled to the other modes.

A slightly more exact estimate of m_1 can be obtained by noting the

difference between the term $\beta + \left(\beta - \frac{1}{N_{BO}} \right) \sum_{n=1}^{M} \frac{H_n}{\Omega_n^2}$ and its correct value of

0.264β (the differences are always small), attributing this error to H_1/Ω_1^2

(H_1/Ω_1^2 is much larger numerically than the other H_n/Ω_n^2), correcting H_1/Ω_1^2

so that the difference is zero, and then using the corrected H_1/Ω_1^2 to calculate

m_1 in Eq. (38).

For example, using the previous results for $N_{BO} = 20$ and $M = 3$:

$H_1 = -1.546$, $H_2 = 0.146$, $H_3 = 0.095$; $I_1 = -0.672$, $I_2 = 0.015$, $I_3 = 0.007$;

$\Omega_1^2 = 1.819$, $\Omega_2^2 = 10.373$, $\Omega_3^2 = 31.797$. Then, $\beta + \left(\beta - \dfrac{1}{N_{BO}}\right) \sum_{n=1}^{3} \dfrac{H_n}{\Omega_n^2} = 0.340$

$+ (0.290)(-0.833) = 0.098$, instead of the exact value of $0.264\beta = 0.090$. Thus,

correcting $H_1/\Omega_1^2 = -0.850$ by -0.008, as outlined above, one finds that

$m_1 = 0.417\pi\rho R_o^3$, $m_2 \approx m_3 \approx 0$ and $m_o = (h/R_o - 0.327)\pi\rho R_o^3$; and $k_1 = 0.760\pi\rho g R_o^2$.

For comparison, when $N_{BO} = \infty$, known results [10] predict that $m_1 = 0.455\pi\rho R_o^3$

and $k_1 = 0.837\pi\rho g R_o^2$. * In Figure 4, the fundamental sloshing mass, m_1, is

shown as a function of the Bond number; in every case, the amount of liquid

participating in the sloshing motion is smaller than that for $N_{BO} = \infty$, and,

in fact, for $N_{BO} = 10$, the sloshing mass is almost 10 percent less than the

high-g case. The spring constant, k_1, is also shown in Figure 4. The amount

of liquid participating in the second and higher modes is very small.

The moment exerted on the tank is caused both by the direct action of

the surface tension and by the sloshing pressures. Taking a reference axis

in an inertial reference frame whose origin coincides with $z = -h$, $r = 0$,

for $t = 0$, in the direction $\theta = \pm\pi/2$ (i.e., the axis is perpendicular to the

excitation), the moment due directly to interfacial forces is

$$M_1 = -\int_0^{2\pi} (h + \beta R_o) \frac{\partial \eta(r = R_o)}{\partial \theta} T \sin\theta \, d\theta$$

---

*The difference between the values of m_1 for $N_{BO} = 20$ and $N_{BO} = \infty$ is sub-
stantially larger than the probable error of $0.008\pi\rho R_o^3$ in the calculations for
$N_{BO} = 20$; this is always the case.

when higher order products of η are neglected. Thus,

$$M_1 = (h + \beta R_o) F_1 = \frac{h + \beta R_o}{N_{BO}} \pi \rho R_o^3 x_o \omega^2 \sin \omega t \sum_{n=1}^{M} \frac{H_n \frac{g}{R_o}}{\omega^2 - \Omega_n^2 \frac{g}{R_o}} \tag{41}$$

The direct contribution of the liquid pressure to the moment is*

$$M_2 = R_o^3 \int_0^{2\pi} \int_{-\frac{h}{R_o}}^{\beta + \epsilon_o} \left(Z + \frac{h}{R_o}\right) [p(R = 1)] \cos \theta \, dZ \, d\theta$$

$$+ R_o^3 \int_0^{2\pi} \int_0^1 R^2 \left[p\left(Z = -\frac{h}{R_o}\right)\right] \cos \theta \, dR \, d\theta \tag{42}$$

The second integral in Eq. (42) is the moment exerted on the <u>bottom</u> of the

tank; since $\Phi \approx 0$ for $Z = -h/R_o$, this integral reduces to $\frac{\pi}{4} \rho R_o^4 x_o \omega^2 \sin \omega t$.

Hence, altogether M_2 is

$$M_2 = \pi \rho R_o^4 x_o \omega^2 \sin \omega t \left\{ \frac{1}{2}\left(\frac{h}{R_o} + \beta\right)^2 - \beta\left(\frac{h}{R_o} + \beta\right) \sum_{n=1}^{M} \frac{H_n \frac{g}{R_o}}{\omega^2 - \Omega_n^2 \frac{g}{R_o}} \right.$$

$$\left. + \omega^2 \sum_{n=1}^{M} \frac{L_n}{\omega^2 - \Omega_n^2 \frac{g}{R_o}} + \frac{1}{4} \right\}$$

where $L_n = \sum_{m=1}^{M} \left(\frac{h}{R_o} + \beta - \frac{1}{\lambda_m}\right) \frac{P_{nm}}{\lambda_m} J_1(\lambda_m) e^{\lambda_m \beta}$. After combining M_1 and

M_2, the total dynamic moment on the tank is:

---

*The contribution arising from the displacement of the entire mass of liquid as a rigid body relative to the inertial frame (which equals $m_T x_o \sin \omega t$) is neglected because it can be computed statically.

$$M = \pi \rho R_o^4 x_o \omega^2 \sin \omega t \left\{ \frac{1}{2}\left(\frac{h}{R_o}+\beta\right)^2 - \left(\beta - \frac{1}{N_{BO}}\right)\left(\frac{h}{R_o}+\beta\right) \sum_{n=1}^{M} \frac{H_n \frac{g}{R_o}}{\omega^2 - \Omega_n^2 \frac{g}{R_o}} \right.$$

$$\left. + \omega^2 \sum_{n=1}^{M} \frac{L_n}{\omega^2 - \Omega_n^2 \frac{g}{R_o}} + \frac{1}{4} \right\} \qquad (43)$$

Using the previous observation that $\beta + \left(\beta - \frac{1}{N_{BO}}\right) \sum_{n=1}^{M} \frac{H_n}{\Omega_n^2} = 0.264\beta$ and

rearranging the terms in a manner similar to that used in Eq. (36), Eq. (43)

is finally written as

$$M = \pi \rho R_o^4 x_o \omega^2 \sin \omega t \left\{ \left(\frac{h}{R_o}+0.264\beta\right) \left[\frac{\frac{h}{R_o}+0.528\beta+0.128\beta^2\frac{R_o}{h}}{2\left(1+0.264\beta\frac{R_o}{h}\right)}\right] \right.$$

$$\left. + (0.25 - 0.3\beta^2) + \omega^2 \sum_{n=1}^{M} \frac{L_n - \left(\beta - \frac{1}{N_{BO}}\right)\left(\frac{h}{R_o}+\beta\right)\frac{H_n}{\Omega_n^2}}{\omega^2 - \Omega_n^2 \frac{g}{R_o}} \right\} \qquad (44)$$

Since the distance from the bottom of the tank to the center-of-mass of the

liquid is*

$$h_{c.m.} = R_o\left[\frac{\frac{h}{R_o}+0.528\beta+0.128\beta^2\frac{R_o}{h}}{2\left(1+0.264\beta\frac{R_o}{h}\right)}\right] \qquad (45)$$

it turns out that Eq. (44) is equivalent to:

---

*This distance equals the distance to the c.m. of the undisturbed liquid in
the linearized approximations used here.

$$M = \pi\rho R_o^4 x_o \omega^2 \sin \omega t \left\{ \frac{m_T h_{c.m.}}{\pi\rho R_o^4} + (0.25 - 0.3\beta^2) \right.$$

$$\left. + \omega^2 \sum_{n=1}^{M} \frac{L_n - \left(\beta - \frac{1}{N_{BO}}\right)\left(\frac{h}{R_o} + \beta\right)\frac{H_n}{\Omega_n^2}}{\omega^2 - \Omega_n^2 \frac{g}{R_o}} \right\} \qquad (46)$$

Carrying out the calculations for the mechanical model, the moment of the system of vibrating masses about the same reference axis is

$$M_{model} = x_o \omega^2 \sin \omega t \left\{ h_o m_o + \sum_{n=1}^{M} h_n m_n + \sum_{n=1}^{M} \frac{m_n g}{\omega_n^2} \right.$$

$$\left. - \omega^2 \sum_{n=1}^{M} \frac{m_n (h_n - g/\omega_n^2)}{\omega^2 - \omega_n^2} \right\} \qquad (47)$$

Since $h_o m_o + \sum_{n=1}^{M} h_n m_n$ is, by definition, equal to $h_{c.m.} m_T$, Eq. (44) and

Eq. (46) give the same resulting moment if m_n, m_o, and ω_n are calculated

as previously indicated and if in addition

$$h_n = -\frac{1}{m_n}\left[L_n - \left(\beta - \frac{1}{N_{BO}}\right)\left(\frac{h}{R_o} + \beta\right)\frac{H_n}{\Omega_n^2}\right]\pi\rho R_o^4 - \frac{R_o}{\Omega_n^2}$$

$$= R_o \left\{ \frac{h}{R_o} - \frac{1}{\Omega_m^2} - \frac{\pi\rho R_o^3}{m_n}\left[\sum_{m=1}^{M}\left(\beta - \frac{1}{\lambda_m}\right)\frac{P_{nm} J_1(\lambda_m) e^{\lambda_m \beta}}{\lambda_m}\right.\right.$$

$$\left.\left. - \beta\left(\beta - \frac{1}{N_{BO}}\right)\frac{H_n}{\Omega_n^2}\right]\right\} \qquad (48)$$

and

$$h_o = \frac{1}{m_o}\left(m_T h_{c.m.} - \sum_{n=1}^{M} m_n h_n\right) \qquad (49)$$

Note, again, that h_n depends only on the nth sloshing mode. Unfortunately, these expressions cannot be simplified a great deal, but for $N_{BO} = \infty$, in which case $\Omega_n^2 = \lambda_n$ and $P_{nm} = 0$ for $n \neq m$, Eq. (48) reduces to

$$h_n = h - \frac{2R_o}{\lambda_n}$$

which is the correct result [10].

Another apparent requirement for moment equality from Eqs. (46) and (47) is

$$\sum_{n=1}^{M} \frac{m_n g}{\omega_n^2} = \left(\frac{1}{4} - 0.3\beta^2\right) \pi \rho R_o^4 \tag{50}$$

When $N_{BO} = \infty$, Eq. (50) is not independent of the previous requirements since

$1/4 = 2 \sum_{n=1}^{\infty} [\lambda_n^2(\lambda_n^2 - 1)]^{-1}$, $\omega^2 = \lambda_n g/R_o$, and $m_n = 2\pi\rho R_o^3 [\lambda_n(\lambda_n^2 - 1)]^{-1}$; hence,

Eq. (50) is satisfied identically [10]. For $\beta \neq 0$, it cannot be proved that Eq. (50) is _not_ an independent requirement; yet, within the accuracy of the numerical examples, it seems that satisfying Eq. (50) is not necessary if m_n, m_o, k_n, h_n, and h_o are calculated by the previous equations; furthermore, the selection of the model parameters would be overdetermined if Eq. (50) were independent. Thus, Eq. (50) will be assumed not to be another independent requirement and henceforth will be neglected.

For the previous numerical example ($N_{BO} = 20$, $M = 3$), it turns out that $h_1 = h_{av} - 1.179R_o$, as compared to $h_1 = h_{av} - 1.086R_o$ for $N_{BO} = \infty$ where h_{av} is defined by $h_{av} = m_T/\pi\rho R_o^2$; thus, the line of action of the spring-mass system is slightly nearer the bottom of the tank than for $N_{BO} = \infty$. The

variation of h_1 with the Bond number is shown in Figure 5. The other spring-mass heights, h_2, h_3, ..., are not shown because the extremely small magnitude of m_2, m_3, ..., prevents their being accurately calculated.

The average liquid depth, h_{av} and the center-of-mass distance, $h_{c.m.}$ are shown in Figure 6; using this information, h_o can be computed in any particular case from Eq. (49) when it is recognized that the products $m_2 h_2$, $m_3 h_3$, ..., can be neglected in comparison to $m_1 h_1$.

III. EXPERIMENTAL APPARATUS AND PROCEDURES

An overall view of the experimental setup is shown in Figure 7a, although the probe used to determine the displacement of the tank (a "Bently" electromagnetic probe) has been removed for the purposes of clarity. A closeup view of the tank and dynamometer system is shown in Figure 7b, which in this case also shows the displacement probe. The tanks shown are made of glass and are approximately 1 in. in diameter; they are attached directly to the flexure arm structure of the dynamometer; semiconductor strain gages (gage factor = 118) are mounted on the flexure arms, which are strips of aluminum 0.0055 in. thick, 0.312 in. wide, and about 7/16 in. long. The dynamometer structure is bolted to a base which is then mounted on the armature of the electrodynamic shaker; this arrangement allows the tanks to be excited in pure translation.

As can be seen in Figure 7b, there are two test tanks. One tank, called the active tank, contains the test liquid, and the other tank, called the balance tank, is used to cancel the inertial signal of the empty active tank by appropriate electrical connections and the adding of balance weights; thus, the signal reaching the oscillograph is that due only to the inertia of the sloshing liquid plus any slight residual forces which could not be cancelled. The electrical leads from the tension and compression sides of the balance tank (the gages marked T_B and C_B in Fig. 8) are connected to the gages from the active tank through a Wheatstone bridge. Details of the wiring and an electrical schematic are shown in Figure 8.

Before each series of tests, the tanks were carefully cleaned in a detergent-and-water solution and rinsed with ethanol and distilled water. In some of the tests for which distilled water was used, the tanks were also cleaned in both a NaOH solution and a hot chromic acid solution. The top of the tank was then covered with a clean plastic wrapper ("Saran Wrap") which was removed only to put in the test liquid. All of the hardware that came into contact with the test liquid was cleaned in the same manner. In this way, the liquid surface was kept free of contamination.

After a set of tanks was installed in the dynamometer rig, the signal from the empty active and the balance tanks was cancelled as nearly as possible by adding tare weights to the balance tank, as described previously. Next, the displacement probe was calibrated by setting known static displacements of the shaker armature with a dial indicator and recording the probe signal on the oscillograph. After this calibration, any residual force signal not entirely cancelled out was recorded by exciting the empty active and balance tanks at various frequencies and amplitudes. A test liquid was then put in the active tank. (The first liquid in each series of tests was always distilled water because this was the most easily contaminated liquid. The other test liquids, methanol and carbon tetrachloride, are both good "cleaners" and not very susceptible to contamination, but, even so, the active tank was always rinsed with distilled water before each change in test liquids. All of the test liquids were reagent grade.) The sloshing forces were next recorded for various excitation amplitudes in a frequency range centered about the fundamental

sloshing frequency.* After the sloshing tests, the residual signals with an empty active tank were again recorded. Then, measured weights (usually rolled up strips of brass shim stock) were put in the active tank and the force output of these weights recorded for various amplitudes and frequencies. Because the amplitude of the actual force exerted by the weights can be calculated exactly ($= \omega^2 x_0$ times mass of the weights), the dynamometer force signal was calibrated by subtracting whatever residual signal was previously noted from the signal of the known weights (taking into account the phase angles of the two signals with respect to the displacement) and plotting the resulting amplitude of the signal against the calculated force. The sloshing force was finally obtained by subtracting the residual signal from the sloshing force signal and comparing the result with the force calibration curves.

The accuracy of the various measurements can be estimated from the following considerations. The excitation frequency could be determined and maintained to the fourth significant digit in the period (in seconds); e.g., a nominal frequency of 5 cps could be set and held with a variation in the true period (0.2 seconds) of about ±0.0003 seconds. The excitation amplitude could be determined and maintained to within ±0.0005 inch. Phase angles between excitation and force traces, which were used only in subtracting the small residual signals from the larger dynamic force signals, could be determined

---

*The forces were quite small so that, to prevent their being masked by external noise, the dynamometer signal was passed through an electronic filter with a band pass of 2 to 30 cps. A plastic dust cover, which can be seen in Figure 7a, was put over the tanks and the dynamometer to prevent stray air currents from giving spurious signals in the frequency range of the band pass of the filter. A clean sinusoidal force signal was usually obtained by these methods.

from the oscillograph records to within about ±20 degrees. The amplitude

of the force signals could be read to about 1 part in 100, with the exception

that for extremely small amplitudes the accuracy was about 1 part in 10.

The deviation of any experimental point in the force calibration was within

±5 percent of the "best-fit" straight line through the data and the zero point.

The height of the liquid in the tank was determined to within ±0.01 in., and

the meniscus height could be determined to about ±0.015 inch. The overall

accuracy of the sloshing force data, after being reduced, is estimated to

be within ±5 percent of their true values.

IV.   TEST RESULTS AND COMPARISON WITH THEORY

A.   Test Results

The main objective of the experimental program was to determine the sloshing force (for incompressible liquids in rigid cylindrical tanks) as a function of the excitation frequency for a band of frequencies centered about the fundamental mode, with the Bond number as a parameter.   No attempt was made to measure the sloshing moments since this would have greatly complicated both the experimental setup and the experimental procedures; for example, not only would residual forces (no liquid in the active tank) have had to be kept as close to zero as practical, but the residual moments would also have had to be cancelled by tare weights.

Four different sized tanks, with diameters from 1.36 in. to 0.384 in., were used in the tests with three different test liquids: distilled water, methanol, and carbon tetrachloride (CCl_4).   Except for one series of tests with a 1.00-in. diameter Lucite tank, all of the tests were run in glass tanks.   As nearly as could be determined from visual observations, the contact angle of all the liquids against the glass tanks were zero degrees, although, with the Lucite tank, the water's contact angle was nearly ninety degrees.   The sloshing motion of the liquids, except as discussed subsequently, appeared to approximate the "free edge" condition very well.

Figures 9 and 10 show the force response curves for CCl_4 and methanol in a 1.36-in. diameter glass tank; the Bond numbers were 175 and 100, respectively.   The solid lines in these figures are faired curves through the experimental data.   There is a pronounced resonance for both liquids in the vicinity

of 5.1 cps, as can be seen from the curves; the curves, in fact, are qualitatively quite similar to resonance curves for ordinary high-g sloshing. Near the resonant frequency, the sloshing is of the rotary or "swirling" type encountered in high-g sloshing [11, 12] in which the surface wave rotates around the tank. The shaded areas shown in the figures indicate in a very crude fashion the swirl-zone boundaries. Once swirling is encountered, the sloshing force, of course, rotates around the tank also, and, thus, the forces in this zone cannot be determined nor the exact resonant frequency found.

The curves for water, methanol, and CCl_4 in a 1.04-in. diameter glass tank are shown in Figures 11, 12, and 13, and for methanol in a 1.00-in. diameter Lucite tank in Figure 14. The methanol and CCl_4 (Bond numbers about 55 and 98, respectively) again display a marked resonance, this time near 5.75 cps because of the smaller tank. However, water (Bond number of 24) responded in a quite different fashion, as shown in Figure 11. The resonance peak, for one thing, is near 6.5 cps instead of the expected value of about 5.75 cps. For another, the response curves appear to be heavily damped; note the difference between the peak force for water and CCl_4 for $x_o \approx 0.005$ inch. Furthermore, the boundaries of the swirling motion, which are highly dependent on the amount of damping present, are not encountered except for large values of the excitation amplitude. The apparent conclusion is that the water's motion is much more highly damped than either the CCl_4 or the methanol. Yet, the viscosity and hence the Reynolds number for all three liquids are approximately the same*; certainly, the differences in the

_____
*$\nu_{H_2O} = 0.0101$ cm^2/sec; $\nu_{CCl_4} = 0.00969$ cm^2/sec; $\nu_{methanol} = 0.0059$ cm^2/sec.

viscous action are not sufficient to explain the discrepancies in the response of the water and that of the other two liquids.* The difference, then, must be due to the water's sticking to the tank walls, and visual observations indicated that, indeed, the water did not slide freely along the tank walls (it was not completely stuck, however), even though extreme care was used to prevent contamination of the water and the tanks (see Section III). The shift in frequency can be explained by a contact line condition of the form $\partial \eta / \partial r = C_1 \eta$, as has been noted before [3], but this equation, if C_1 is a numerical constant, does not seem able to explain the additional damping caused by "sticking." The entire subject of contact angle hysteresis and surface wave damping has recently been reviewed by Miles [13]; he points out that the important physical processes are far from being fully understood.

The water behaved in the same anomalous manner in the other glass tanks, and, since the interest here is in the "free edge" condition, the other response curves for water are not shown.

The response of methanol in a 1.00-in. diameter Lucite tank is shown in Figure 14; it is quite similar to that shown in Figure 12 for a 1.04-in. diameter glass tank. Because of this, and because water has almost a ninety degree contact with Lucite and CCl_4 attacks it, the tests with Lucite tanks were not pursued further.

Curves for methanol and CCl_4 in a 0.688-in. diameter glass tank (Bond numbers 26 and 45) and for CCl_4 in a 0.384-in. diameter glass tank (Bond

*The shift in resonant frequency because of the lower Bond number of the water is not nearly enough to explain the observed frequency shift. See Figure 2.

number 14) are shown in Figures 15, 16, and 17. In these tests, the Bond number is small enough that the interfacial forces are almost as important as the body forces. It can be seen that a pronounced resonance still exists.

B.   Comparison with Theory

The experimental value of the natural frequency is determined from each response curve by assuming it is halfway between the swirl boundaries for the lowest excitation amplitude; this is not an exact procedure, of course. These values are compared with the theoretical predictions in Figure 2. There is considerable scatter of the data about the theoretical curve, but the general trend of the data and the theory is in agreement. In particular, the experimental frequencies, except for $N_{BO} = 14$, are below the high-g limit as the theory predicts. In fact, for several cases, the high-g theoretical frequency lies to the right of the observed swirl boundaries, especially for the higher Bond numbers, whereas the true natural frequency must lie within the swirl region.

Comparison of the theoretical values of β and the observed value of the meniscus height at the wall agree fairly well, but the inaccuracies in measuring the meniscus (± 0.015 in.) make quantitative comparisons very difficult. For example, with $N_{BO} = 14$, the meniscus height is about 0.07 in. in the 0.384-in. diameter tank; this gives a value of $\beta \approx 0.365$ compared to the theoretical prediction of 0.442.

The force response of the proposed mechanical model, with only the fundamental sloshing mass included, is compared with the experimental results in Figures 18 through 23. The solid lines in the figures are the

theoretical predictions, and the small squares and circles indicate actual experimental data taken from the previous curves. The ordinate and abscissa scales deliberately have not been nondimensionalized in order to facilitate direct comparisons. In these curves, the excitation amplitude, x_o, for use in the theory has been adjusted within the ± 0.0005-in. accuracy limits mentioned in Section III until the model and the test results agree at the lowest experimental frequency below the resonance; at this frequency, the force is almost entirely equal to total liquid mass times acceleration (i.e., no magnification due to resonance), and, hence, adjusting x_O can be interpreted as mainly accounting for inaccuracies in measuring both x_o and the force amplitude. The adjustments in x_O are relatively small, and all the curves in Figures 9 through 23 have been labeled with these adjusted values. With this exception, it can be seen that the mechanical model and the test results agree very well, especially for that part of the response curve for frequencies below the natural frequency. The upper part of the response curves do not agree quite so well, but at least part of this discrepancy is caused by the influence of higher order modes, which are not included in the single sloshing-mass model used to derive the theoretical curves.

There are more serious discrepancies between theory and experiment for the smallest Bond number tested, $N_{BO} = 14$. The comparison is shown in Figure 23. If the theoretical natural frequency, $\Omega_1^2 = 1.841$ or $f_1 = 9.66$ cps, is used in the mechanical model, the predicted forces near resonance are much too large in comparison to the test results. However, if the experimental natural frequency, $f_1 = 9.80$ cps, is used in the model, the predicted

forces and the observed forces agree considerably better. It appears from this, then, that the theoretical calculations have not converged to the proper values for Bond numbers near 10. Perhaps by retaining more terms in the potential and wave height equations, this situation could be corrected.

The actual damping was not determined in the tests or used in the theory, but visual observations of the number of cycles required for the sloshing to decay indicated that the total damping was not large (except for the water); this is verified by the good comparison between the idealized theory and the test results. Also, by using the well-established equation for large tanks [14]

$$\delta = 4.96 \ \nu^{1/2} R_o^{-3/4} g^{-1/4}$$

where δ is the log decrement, it is found that, for the smallest (0.384 in.) diameter tank, $\delta \approx 0.097$ to 0.13, and that, for the largest (1.36 in.) diameter tank, $\delta \approx 0.04$ to 0.05 for the methanol and CCl_4. While these are larger values of the log decrement than are usually employed in sloshing tests, they are still not so large as to affect materially either the natural frequency or the force response, with the possible exception that the boundaries for swirling motion are wider in the present tests than are found in tests with larger tanks. Thus, the liquid damping is not considered to be a serious limitation in small-model testing.

V. CONCLUSIONS

This study of lateral sloshing for moderately small Bond numbers has revealed a number of interesting features. The analysis shows that the fundamental sloshing frequency for $10 \leq N_{BO} \leq 100$ is always less than the high-g limit of $\omega_1 = (1.841 \, g/R_o)^{1/2}$ if the liquid's contact angle is zero and if the liquid obeys the "free edge" contact line condition. The amount of liquid taking part in the sloshing motion is also less than the high-g limit; this is a reasonable result because, for the same size tank and the same total amount of contained liquid, more of the liquid is in contact with the walls for small Bond numbers than for large Bond numbers; thus, more of the liquid must follow the motion of the tanks, i.e., more of the liquid must be assigned to the rigid mass, m_o, and less to the sloshing mass, m_1, in the mechanical model. The sloshing masses, moreover, are located slightly nearer the bottom of the tank than for $N_{BO} = \infty$.

The experimental tests have verified the force response of the proposed mechanical model with about the same degree of accuracy as similar mechanical models for high-g sloshing. There is some doubt about the natural frequency for $N_{BO} \approx 10$, but, in general, the correlation between theory and experiment is good. The experiments, furthermore, have demonstrated that it is possible to simulate low-gravity sloshing (i.e., sloshing with small Bond numbers) by the use of small models and still get usable results for the sloshing forces and frequencies. The amount of damping with such small tanks did not appear to be critical. However, considerable care must be used in these

kinds of tests to insure that the tanks are very clean and the liquids pure;

also, test liquids and tank materials must be chosen which will duplicate the

desired conditions of "free edge," "partially stuck edge," or "stuck edge"

contact lines.

VI. ACKNOWLEDGEMENT

LIST OF REFERENCES

1. Habip, L. M., "On the Mechanics of Liquids in Subgravity, " Astronautica Acta, 11, No. 6, pp. 401-409 (1965).

2. Reynolds, W. C., Saad, M. A., and Satterlee, H. M., "Capillary Hydrostatics and Hydrodynamics at Low-g, " TR LG-3, Dept. of Mech. Eng., Stanford University, September 1, 1964.

3. Satterlee, H. M., and Reynolds, W. C., "The Dynamics of the Free Liquid Surface in Cylindrical Containers under Strong Capillary and Weak Gravity Conditions, " TR LG-2, Dept. of Mech. Eng., Stanford University, May 1, 1964.

4. Benedikt, E. T., "A Study of Propellant Behavior at Zero Gravity, " Final Report, Contract NAS8-11097, North American Aviation, Inc., Space and Information Systems Division, April 15, 1966.

5. Ryan, R. S., and Buchanan, H., "An Evaluation of the Low G Propellant Behavior of a Space Vehicle During Waiting Orbit, " NASA TM X-53476, June 22, 1966.

6. Swalley, F. E., Platt, G. K., and Hastings, L. J., "Saturn V Low-Gravity Fluid Mechanics Problems and Their Investigation by Full-Scale Orbital Experiment, " Fluid Mechanics and Heat Transfer under Low Gravity, Proceedings of the 1965 Symposium sponsored by U.S.A.F. Office of Scientific Research and Lockheed Missiles and Space Company, ed. H. Cohen and M. Rogers. No publisher given. pp. 1-1 to 1-24.

7. Satterlee, H. M., and Chin, J. H., "Meniscus Shape under Reduced-Gravity Conditions, " Fluid Mechanics and Heat Transfer under Low Gravity, Proceedings of the 1965 Symposium sponsored by U.S.A.F. Office of Scientific Research and Lockheed Missiles and Space Co., ed. H. Cohen and M. Rogers. No publisher given. pp. 13-1 to 13-24.

8. Handbook of Mathematical Functions, ed. by M. Abramowitz and L. A. Stegun. National Bureau of Standards, Applied Mathematics Series 55, Washington, D. C., June 1964.

9. Benjamin, T. B., and Ursell, F., "The Stability of a Plane Free Surface of a Liquid in Vertical Periodic Motion, " Proc. Royal Soc. (London), A225, pp. 505-515 (1954).

10. Bauer, H. G., "Fluid Oscillations in the Containers of a Space Vehicle and Their Influence Upon Stability, " NASA TR R-187, February 1964.

11.   Hutton, R. E., "An Investigation of Resonant, Nonlinear Nonplanar Free Surface Oscillations of a Liquid, " NASA TN D-1870, May 1963.

12.   Abramson, H. N., Chu, W.-H., and Kana, D. D., "Some Studies of Nonlinear Lateral Sloshing in Rigid Containers, " Final Report, Contract NASr-94(03), Southwest Research Institute, December 1964 (also to appear in December 1966 Journal of Applied Mechanics).

13.   Miles, J. W., "Damping of Gravity Waves by Surface Films, " Sixth Symposium on Naval Hydrodynamics, Paper 23, Volume II, Washington, D.C., September 1966.

14.   Stephens, D. G., Leonard, H. W., and Perry, T. W., "Investigation of the Damping of Liquids in Right-Circular Cylindrical Tanks, Including the Effects of a Time-Variant Liquid Depth, " NASA TN D-1367, July 1962.

APPENDIX A

DEFINITION OF FOURIER-BESSEL COEFFICIENTS

The constants, or Fourier-Bessel coefficients, in Eqs. (21) and (22) are:

$$C1_{nm} = \frac{2\lambda_n^2}{(\lambda_n^2 - 1)[J_1(\lambda_n)]^2} \int_0^1 R \left\{ -\lambda_m J_1(\lambda_m R) \right.$$

$$\left. + \frac{3\beta R^2}{2(1 - R^3)^{1/2}} J_1'(\lambda_m R) \right\} J_1(\lambda_n R) e^{\lambda_m \beta [1 - (1 - R^3)^{1/2}]} dR$$

$$C2_{nm} = \frac{2\lambda_n^2}{(\lambda_n^2 - 1)[J_1(\lambda_n)]^2} \int_0^1 R J_1(\lambda_m R) J_1(\lambda_n R) e^{\lambda_m \beta [1 - (1 - R^3)^{1/2}]} dR$$

and

$$C3_{nm} = \frac{2\lambda_n^2}{(\lambda_n^2 - 1)[J_1(\lambda_n)]^2} \int_0^1 \frac{R}{(N_{BO}) \left(1 - R^3 + \frac{9}{4} \beta^2 R^4 \right)^{3/2}}$$

$$\times \left\{ (1 - R^3)^{3/2} \lambda_m^2 J_1(\lambda_m R) + \frac{9}{4} \beta^2 R^2 (1 - R^3) J_1(\lambda_m R) \right.$$

$$\left. + \left[\frac{9\beta^2 R^3 (1 - 0.25 R^3)(1 - R^3)^{1/2}}{\left(1 - R^3 + \frac{9}{4} \beta^2 R^4 \right)^{3/2}} \right] J_1'(\lambda_m R) \right\} J_1(\lambda_n R) \, dR$$

APPENDIX B

ILLUSTRATIONS
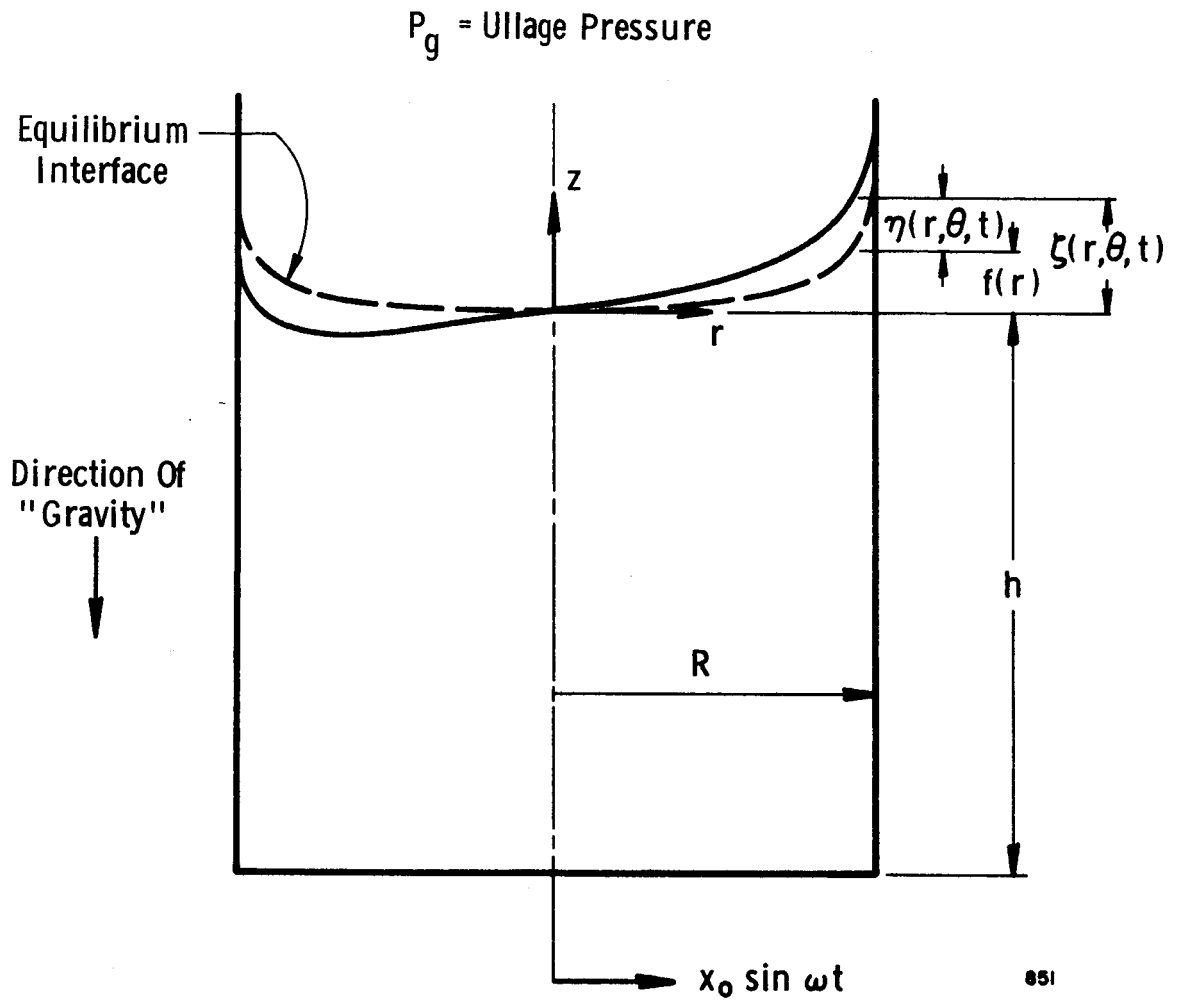
Figure 1. Cylindrical Tank And Coordinate System
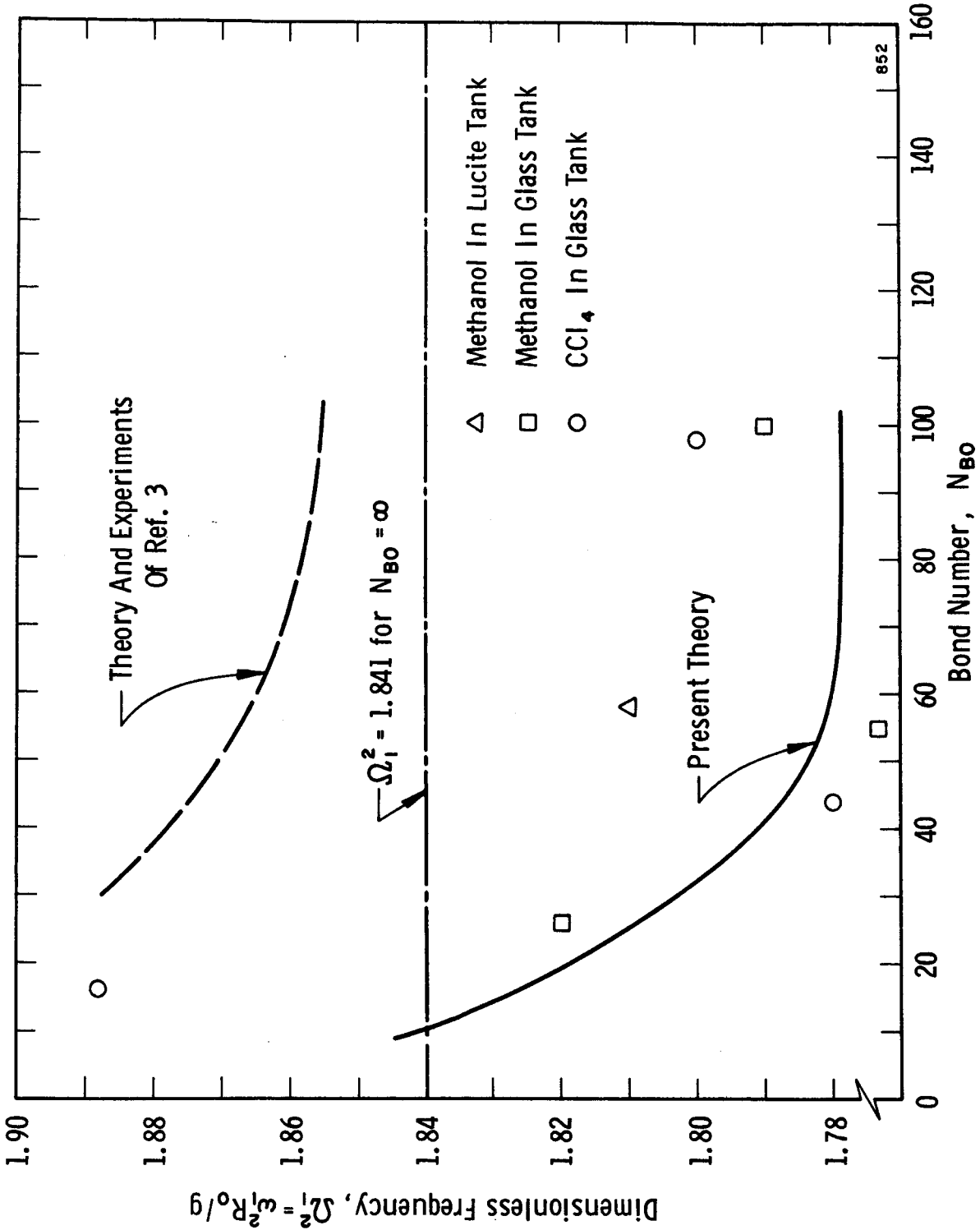
Figure 2. Natural Frequency Of Fundamental Mode

Legend (within figure):

△ Methanol In Lucite Tank
□ Methanol In Glass Tank
○ CCl_4 In Glass Tank

Theory And Experiments Of Ref. 3

$\Omega_i^2 = 1.841$ for $N_{BO} = \infty$

Present Theory

Bond Number, N_{BO}

Dimensionless Frequency, $\Omega_i^2 = \omega_i^2 R_o / g$

852
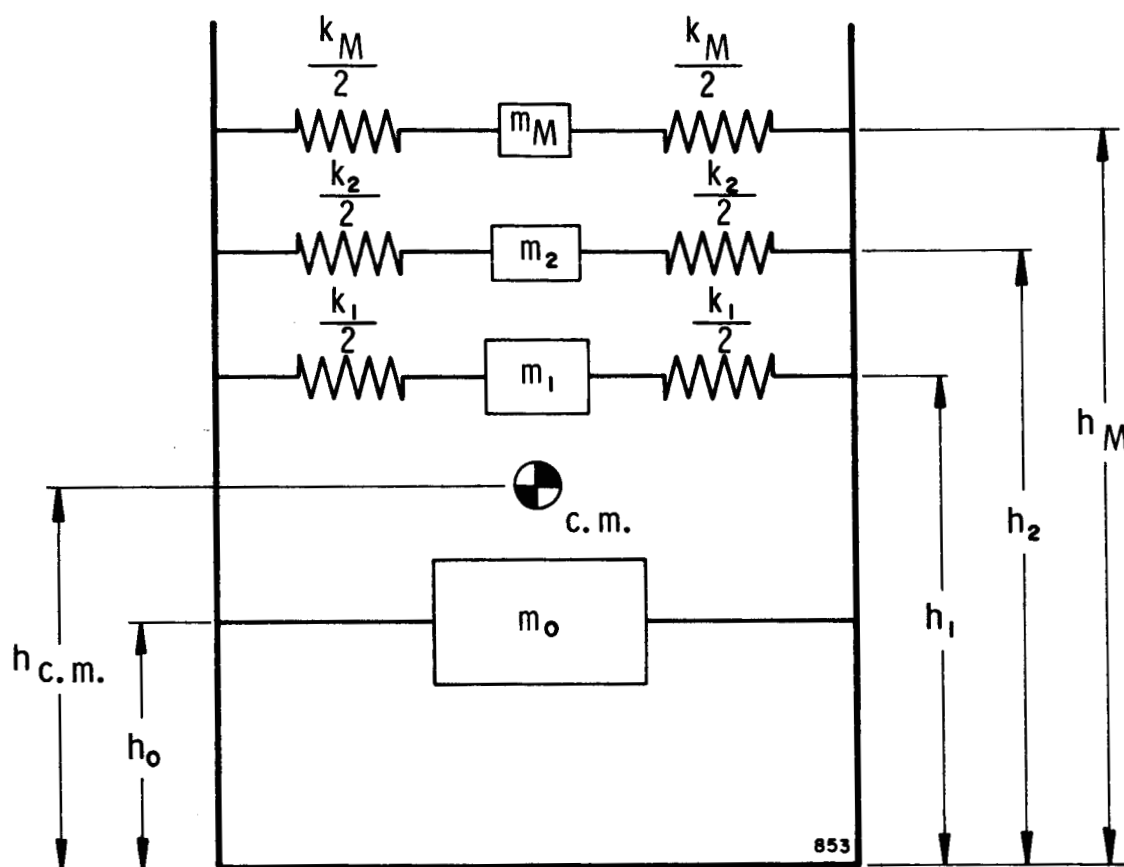
Figure 3. Schematic Of Mechanical Model
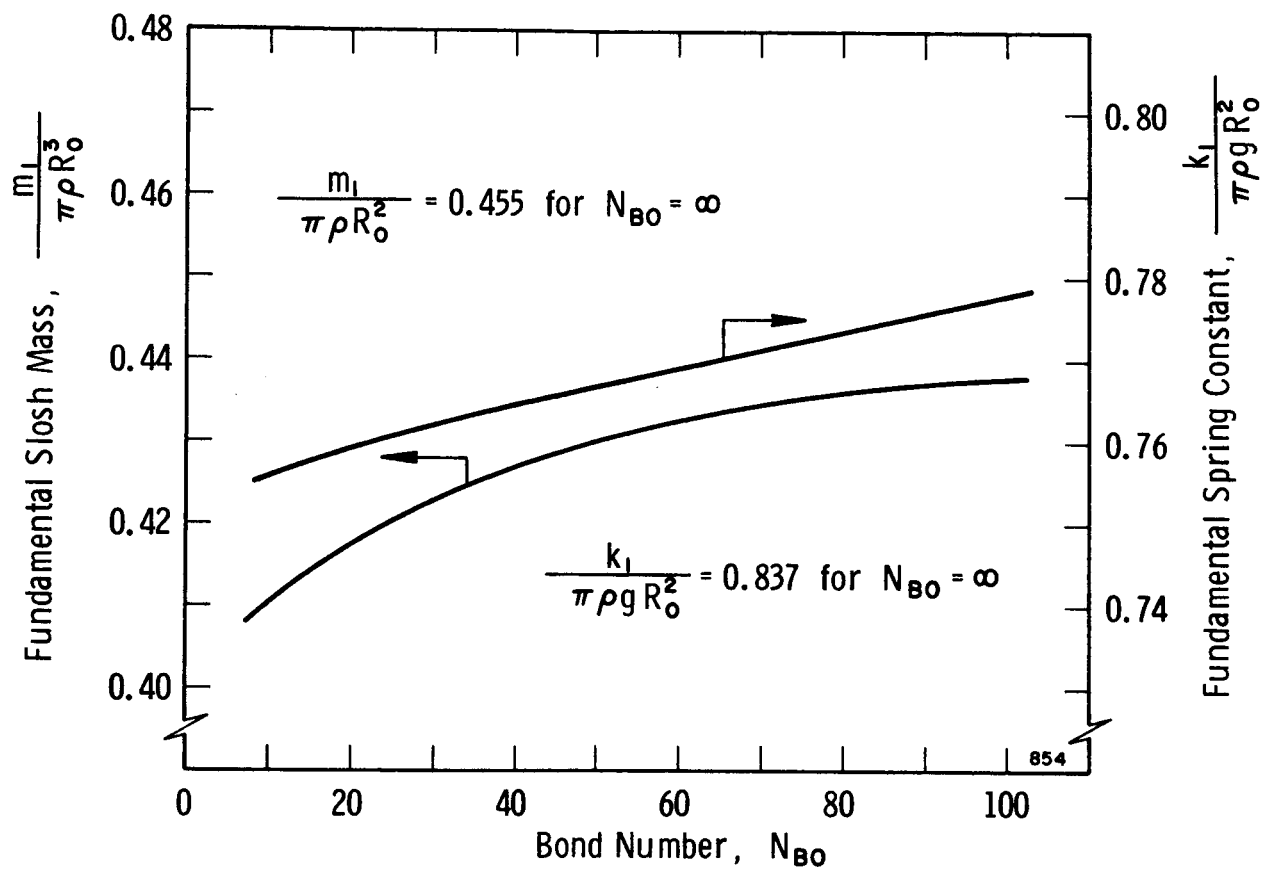
Figure 4. Fundamental Slosh Mass And Spring Constant

The y-axis is labeled "Height Of Slosh Mass Above Bottom, $\dfrac{h_{av} - h_1}{R_0}$" with values 1.12, 1.16, 1.20, 1.24 and 0.

The x-axis is labeled "Bond Number, N_{BO}" with values 0, 20, 40, 60, 80, 100.

On the graph:

$$\frac{h_{av} - h_1}{R_0} = 1.086 \text{ for } N_{BO} = \infty$$

855
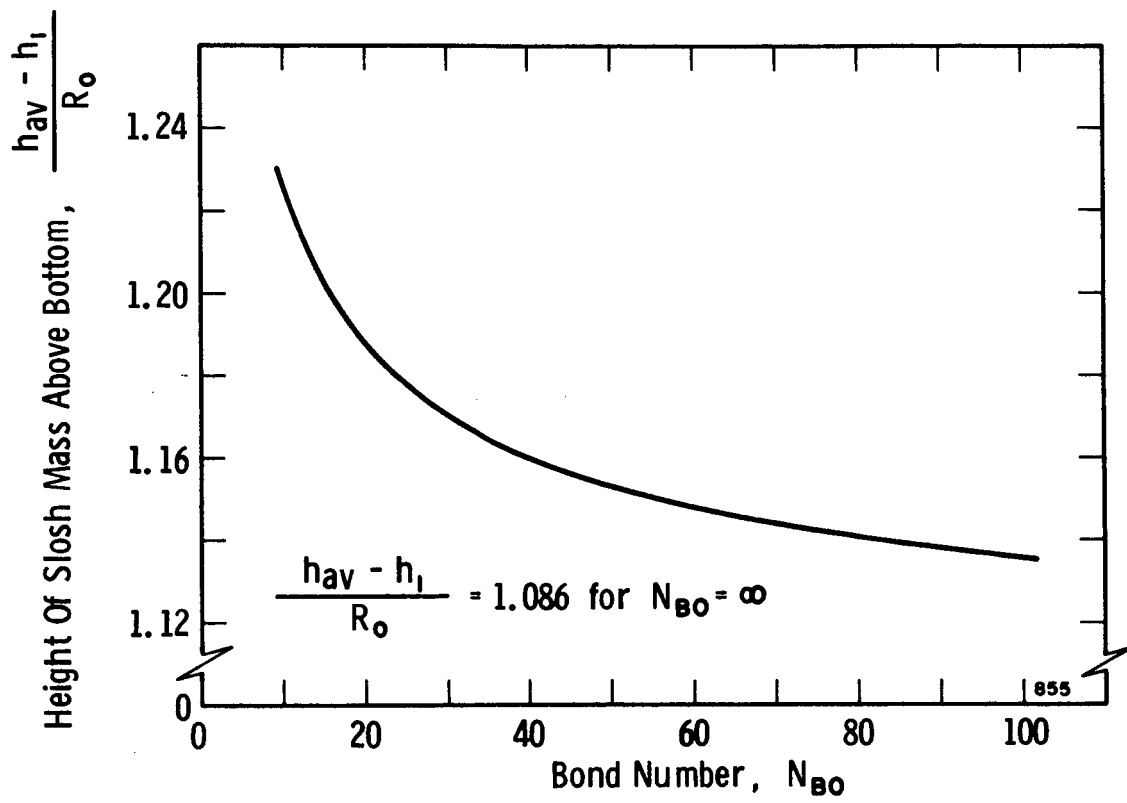
Figure 5. Height Of Fundamental Slosh Mass Above
Bottom Of Tank
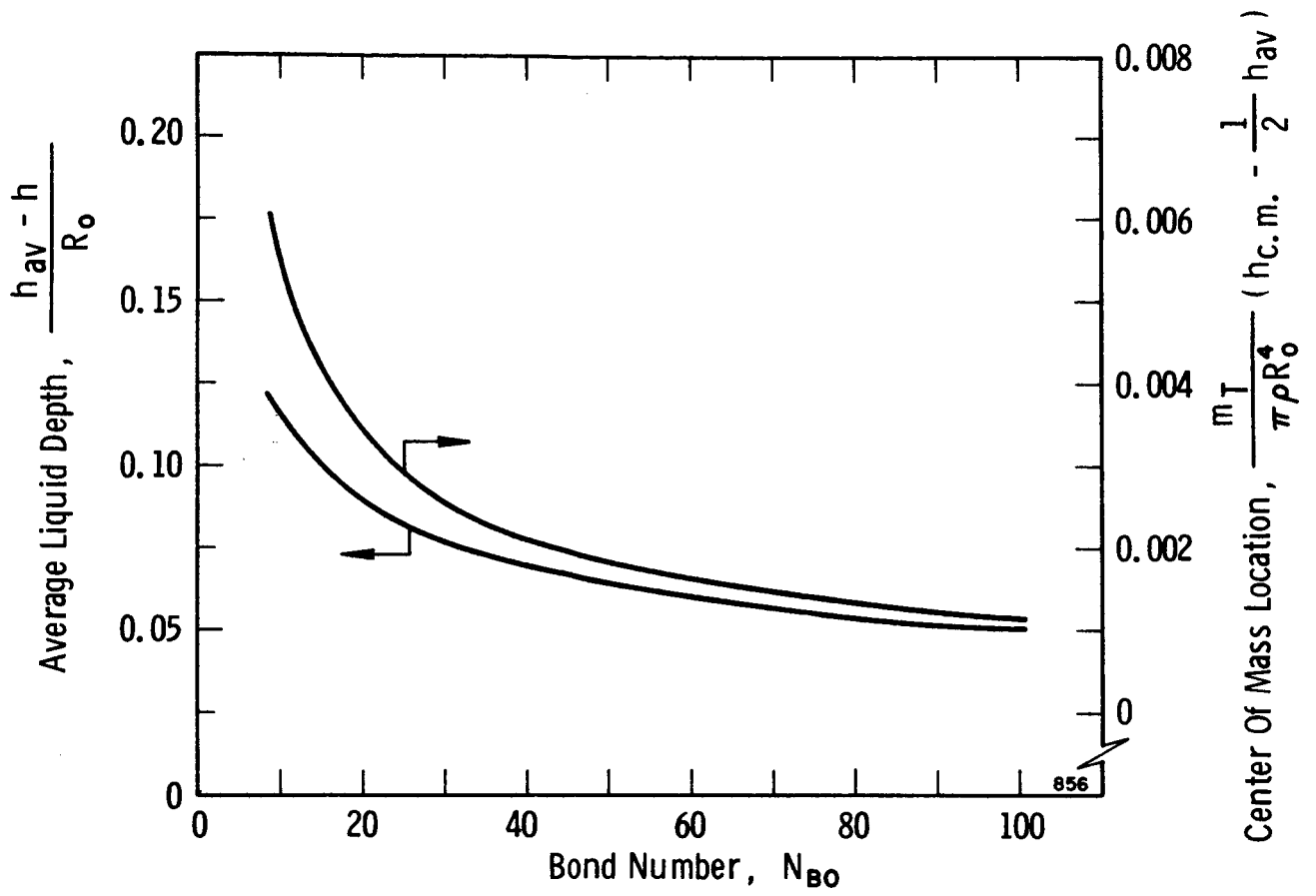
Figure 6. Average Liquid Depth And Center-Of-Mass Location
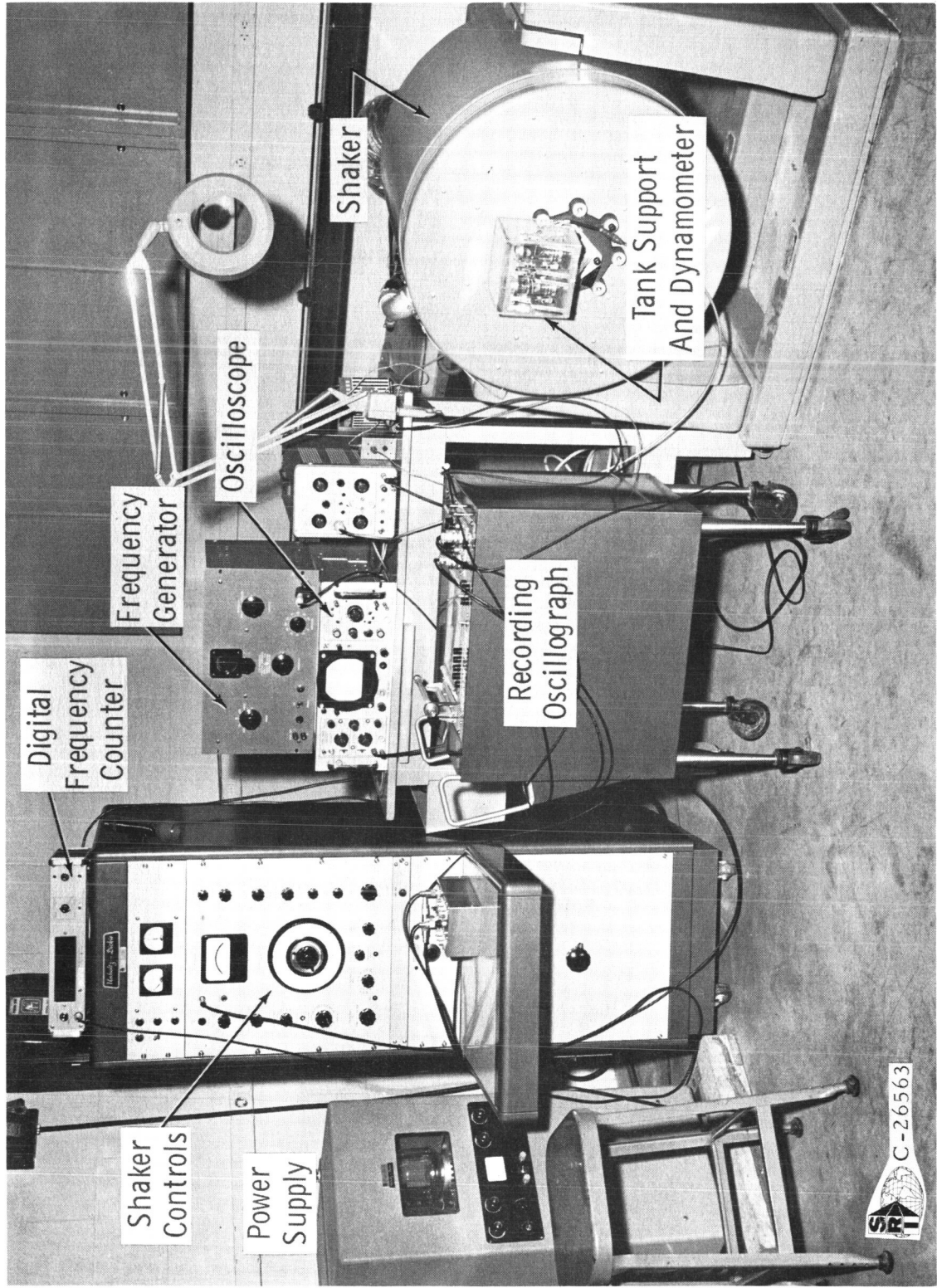
Figure 7a. View Of Experimental Apparatus
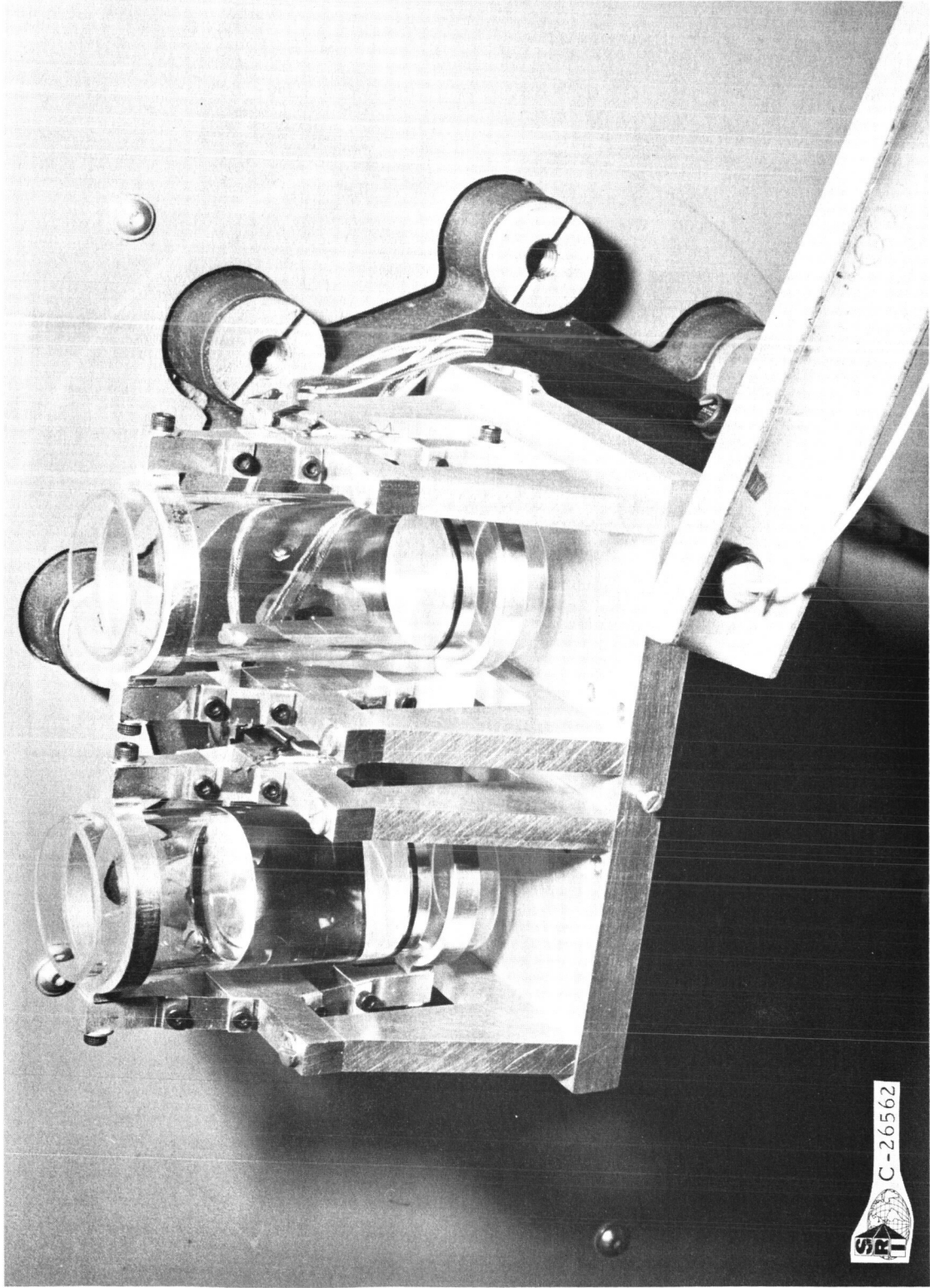
Figure 7b. View Of Glass Tanks And Dynamometer

C-26562
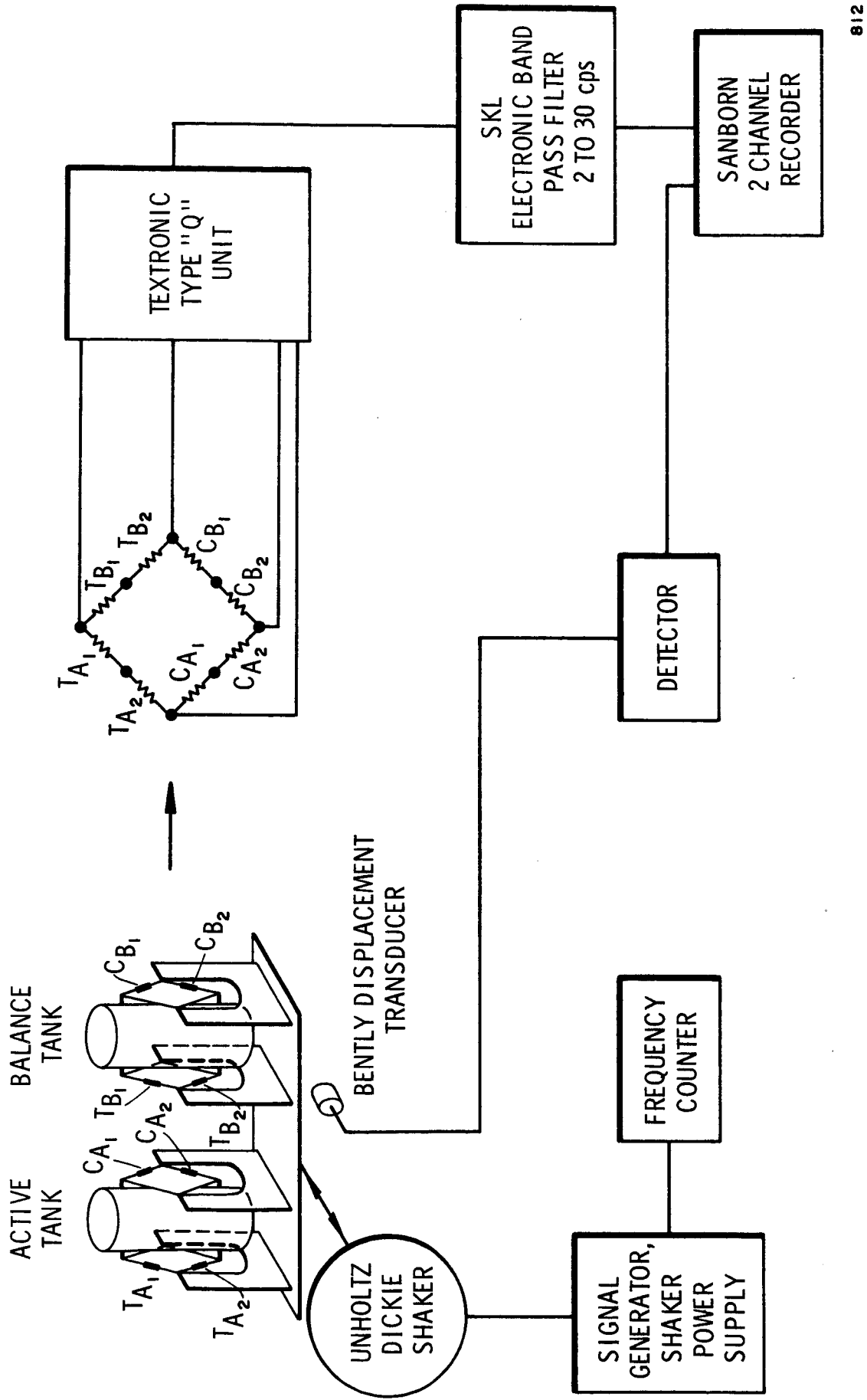
Figure 8. Schematic Of Electrical Wiring

812

ACTIVE TANK

BALANCE TANK

C_{A_1} T_{B_1}

C_{A_2}

C_{B_1}

C_{B_2}

T_{A_1}

T_{A_2}

T_{B_2}

UNHOLTZ DICKIE SHAKER

BENTLY DISPLACEMENT TRANSDUCER

TEXTRONIC TYPE "Q" UNIT

T_{B_1} T_{B_2}

C_{B_1}

T_{A_1}

C_{B_2}

T_{A_2}

C_{A_1}

C_{A_2}

SKL ELECTRONIC BAND PASS FILTER 2 TO 30 cps

SANBORN 2 CHANNEL RECORDER

DETECTOR

FREQUENCY COUNTER

SIGNAL GENERATOR, SHAKER POWER SUPPLY
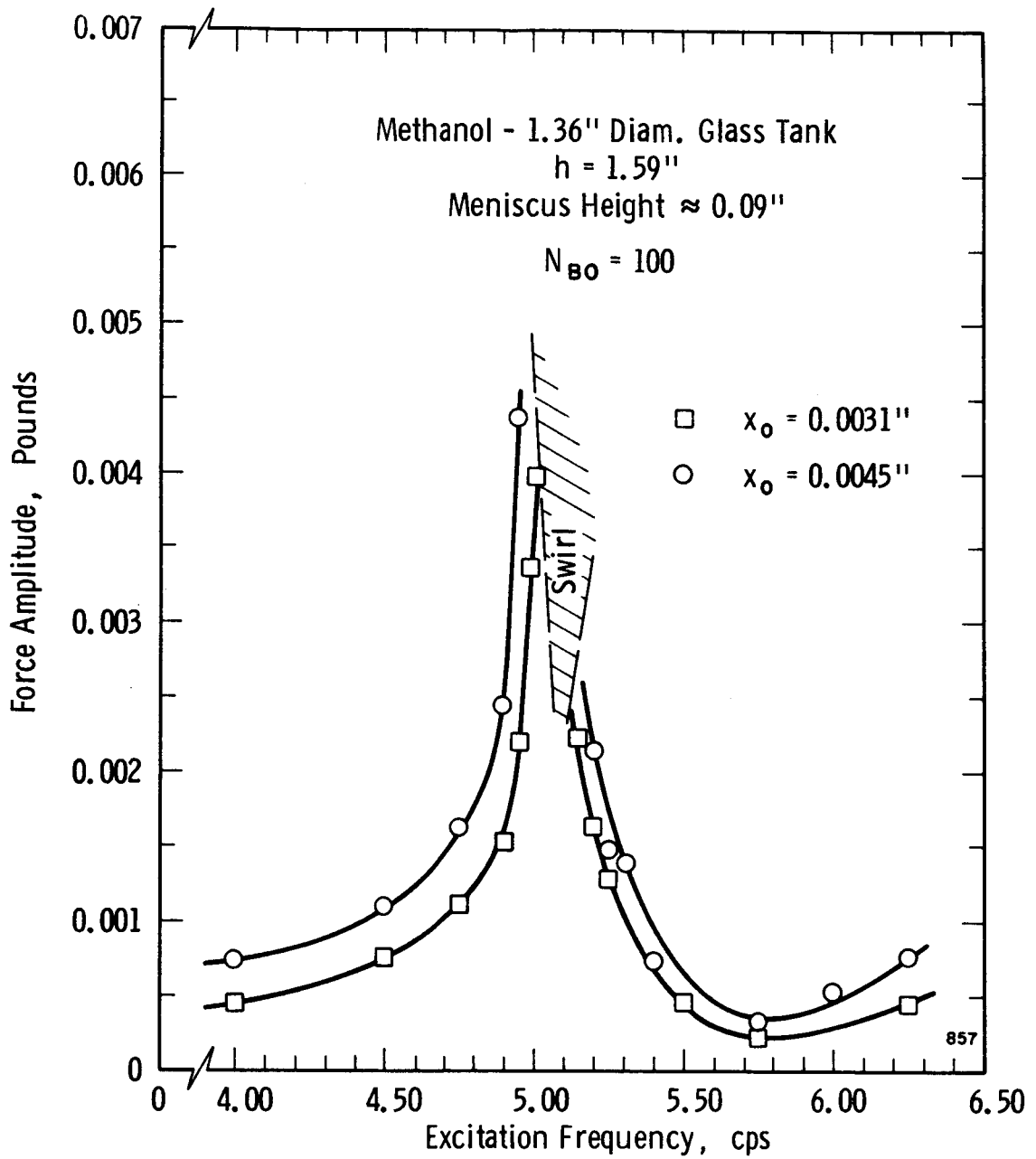
Figure 9.   Response Curve For Methanol,   Bond Number = 100
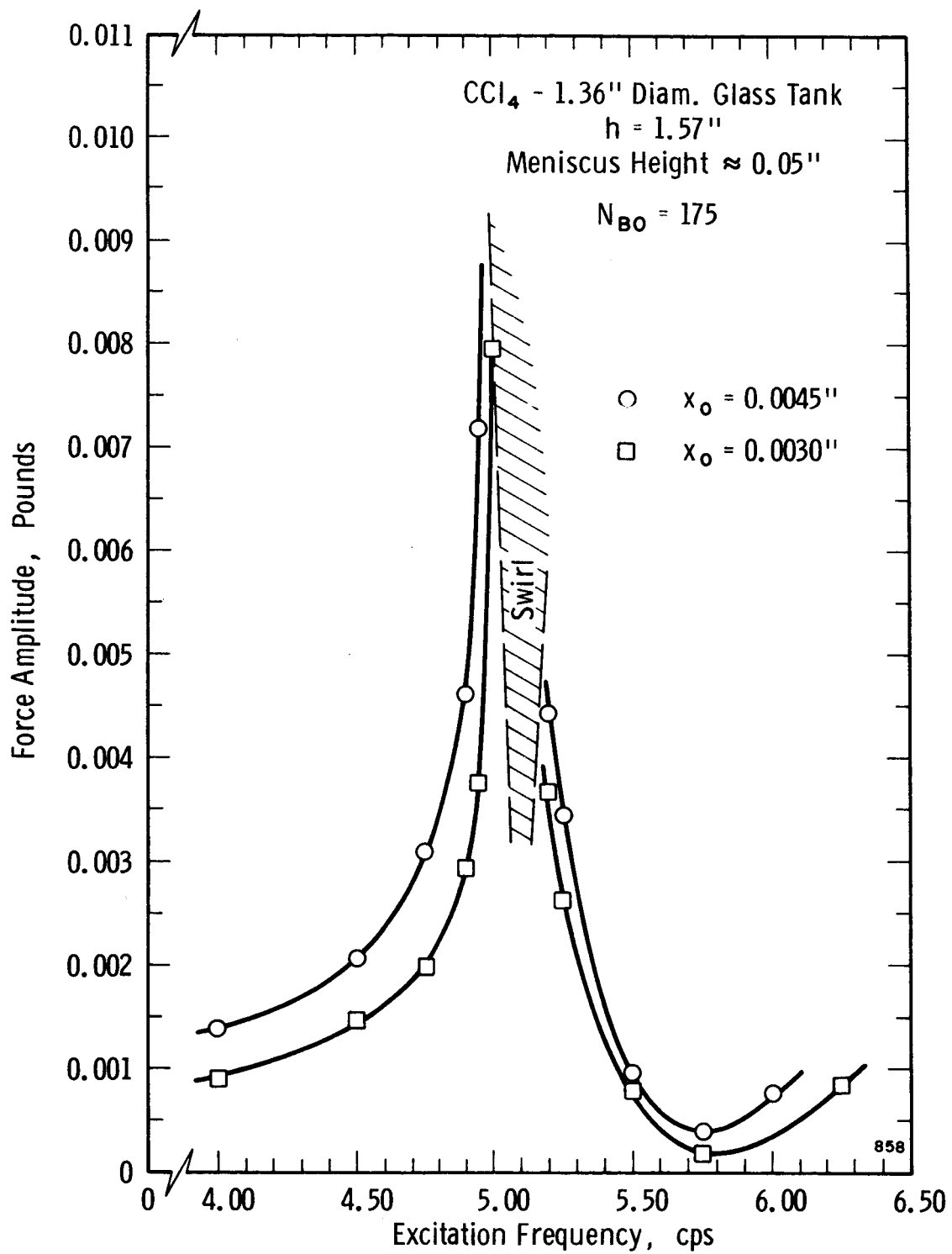
Figure 10.   Response Curve For Carbon Tetrachloride, Bond Number = 175
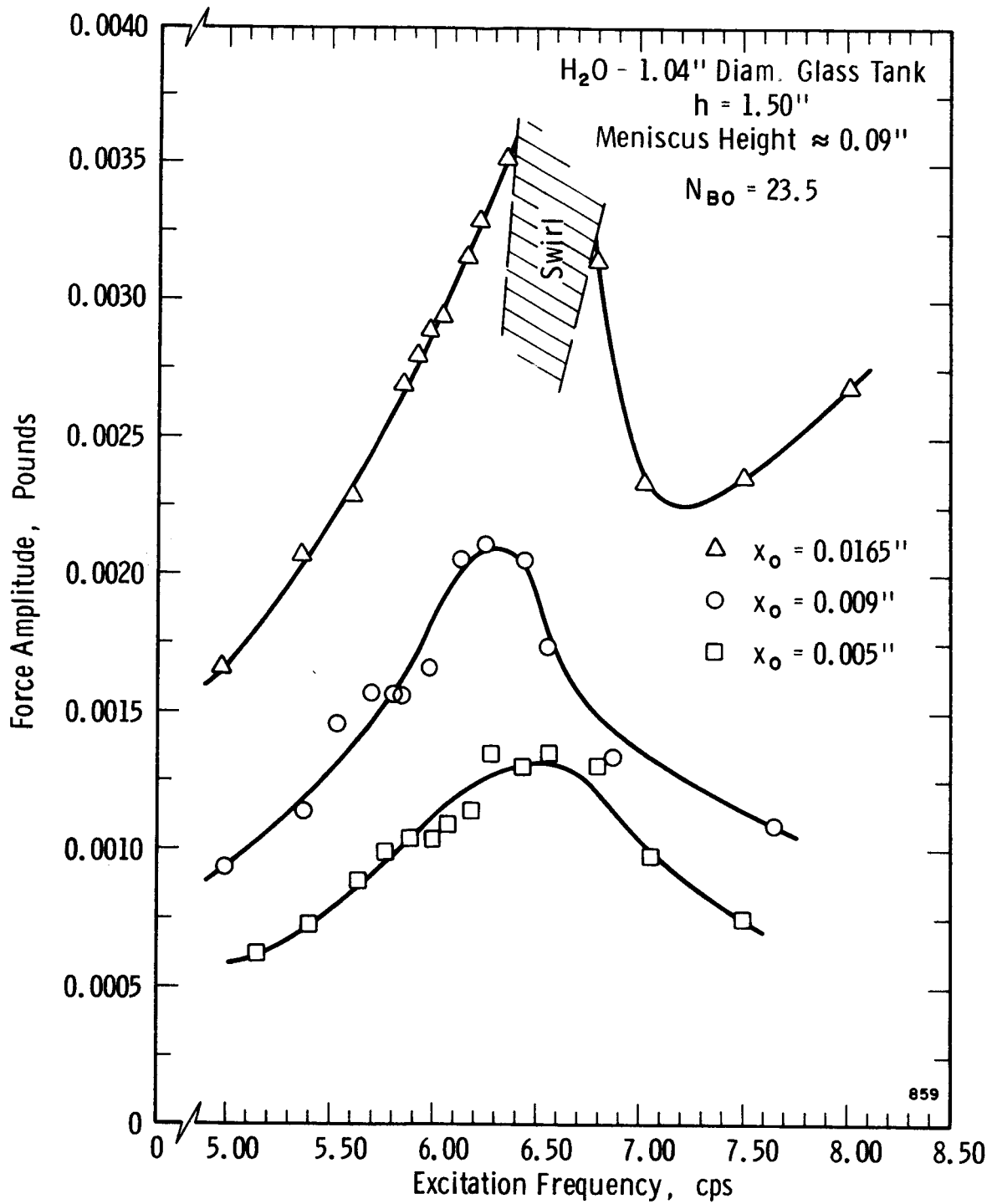
Figure 11. Response Curve For Water, Bond Number = 23.5
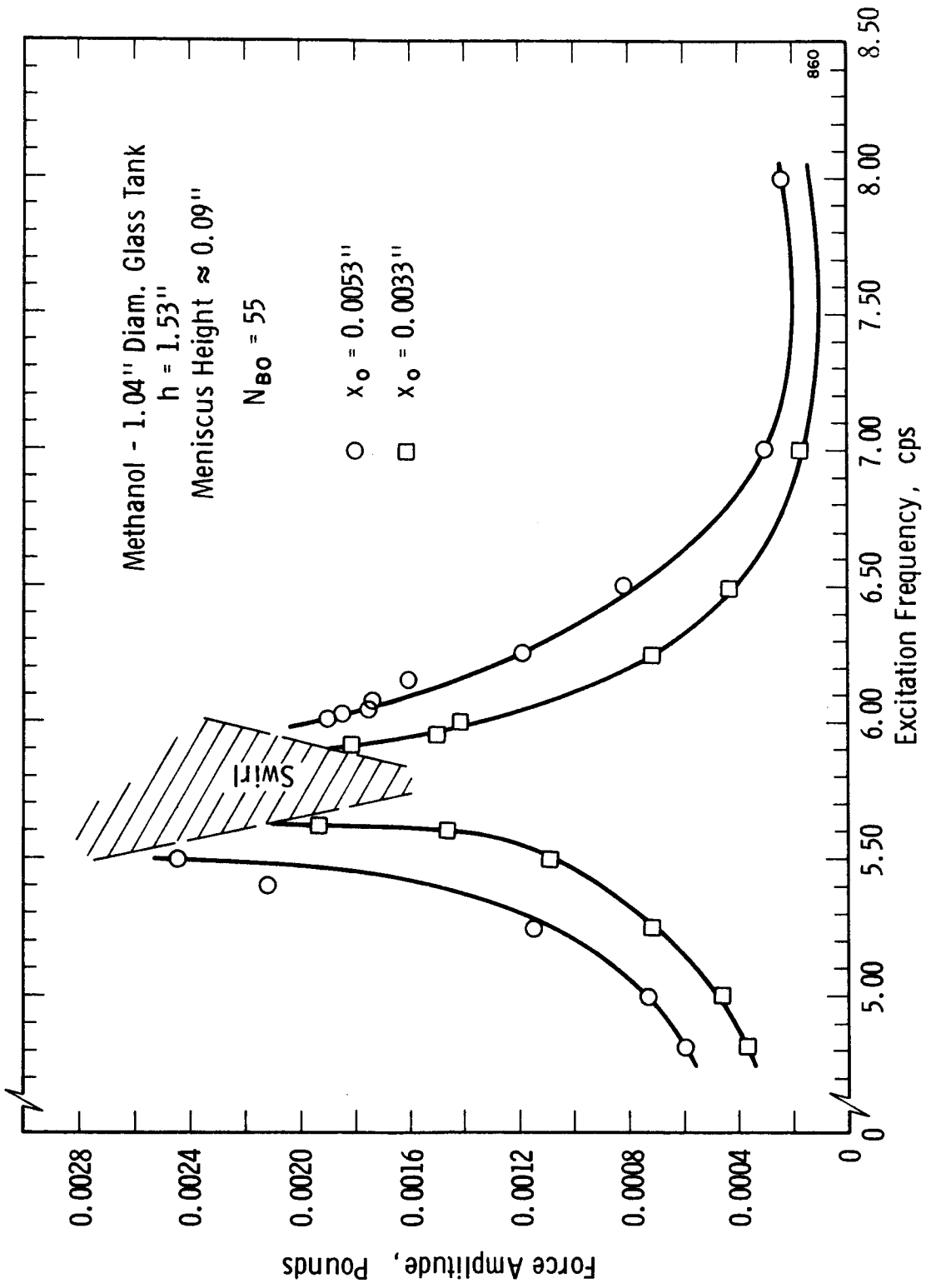
Figure 12.   Response Curve For Methanol, Bond Number = 55
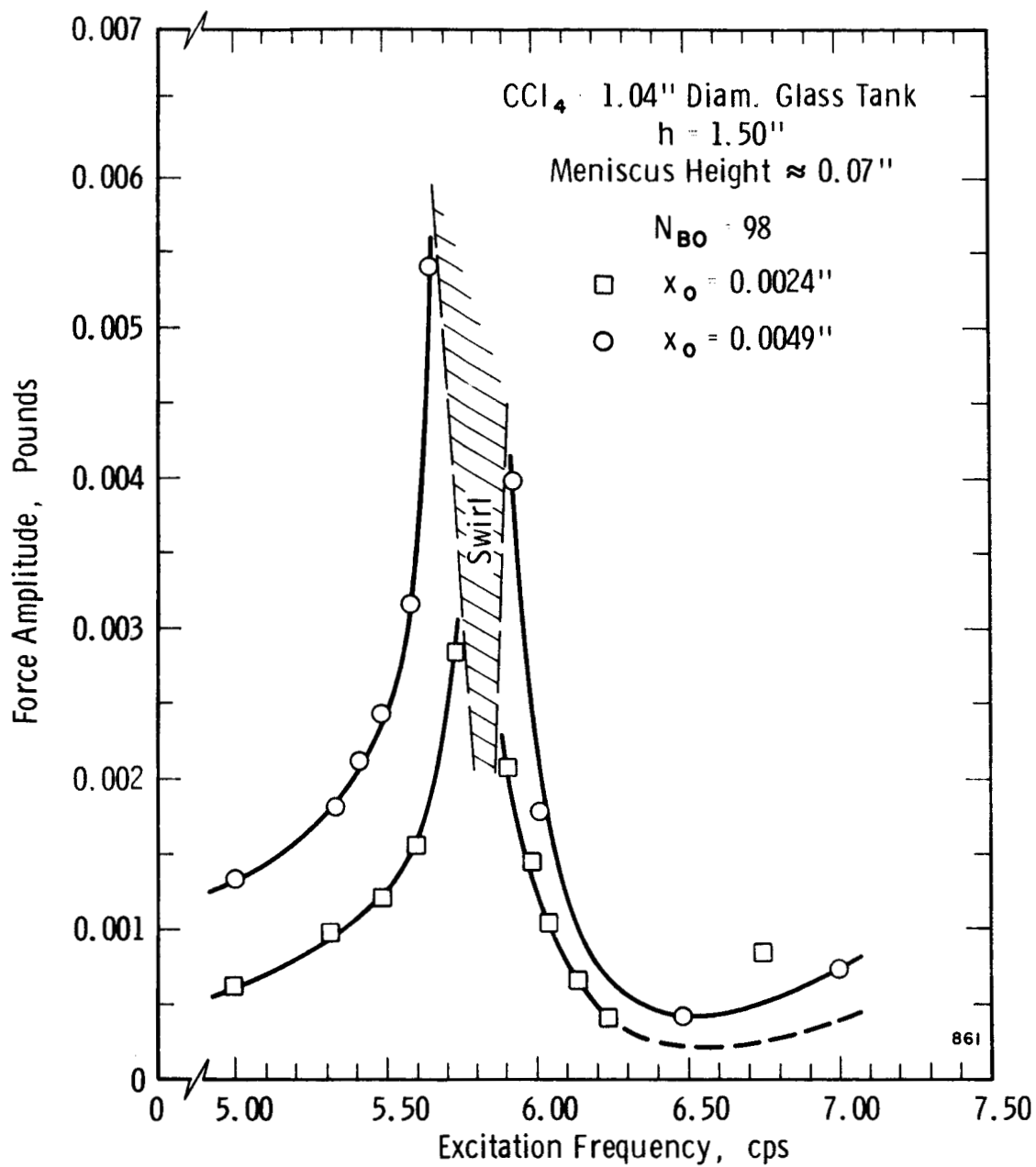
Figure 13. Response Curve For Carbon Tetrachloride, Bond Number = 98
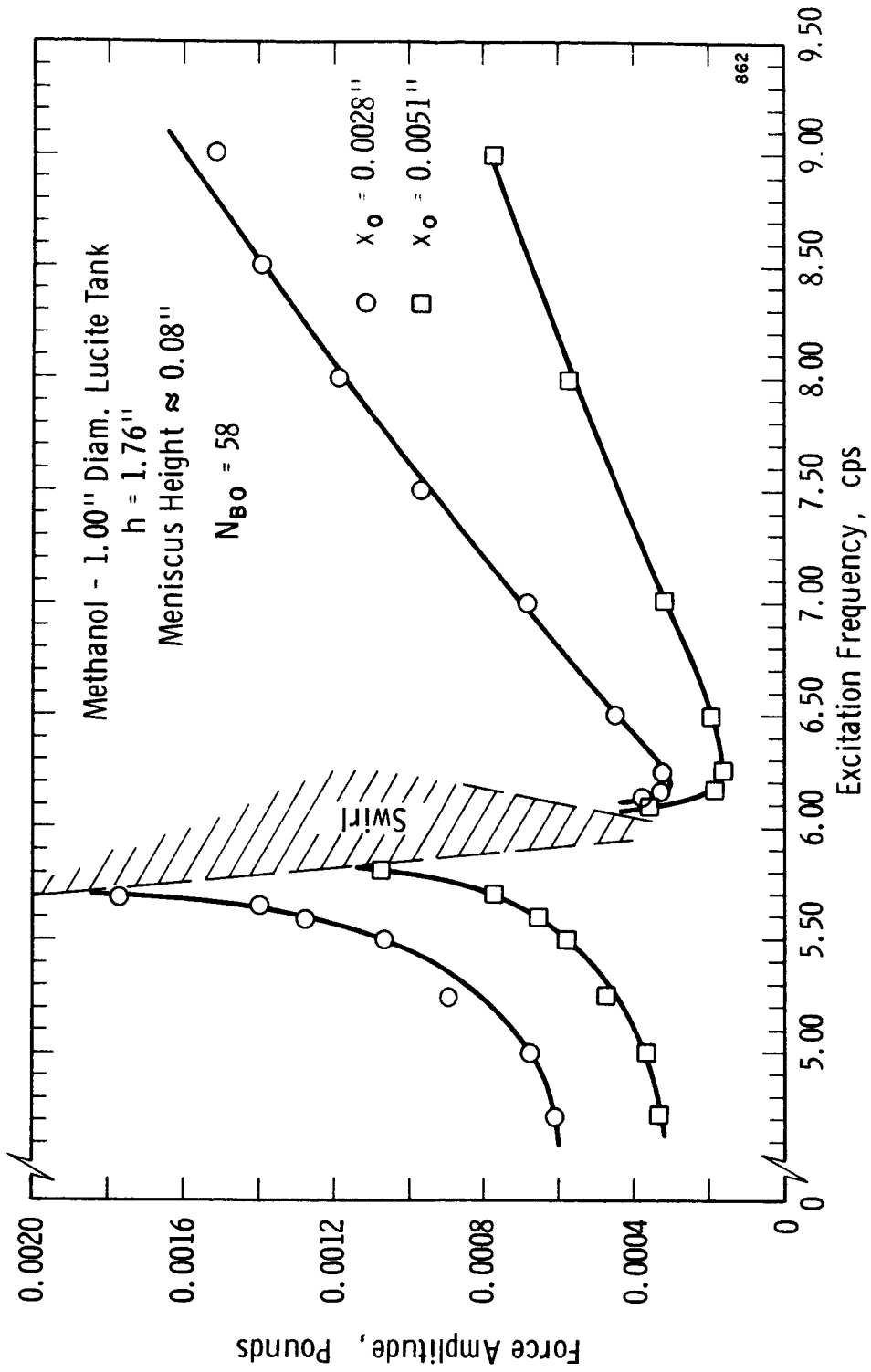
Figure 14.   Response Curve For Methanol, Bond Number = 58
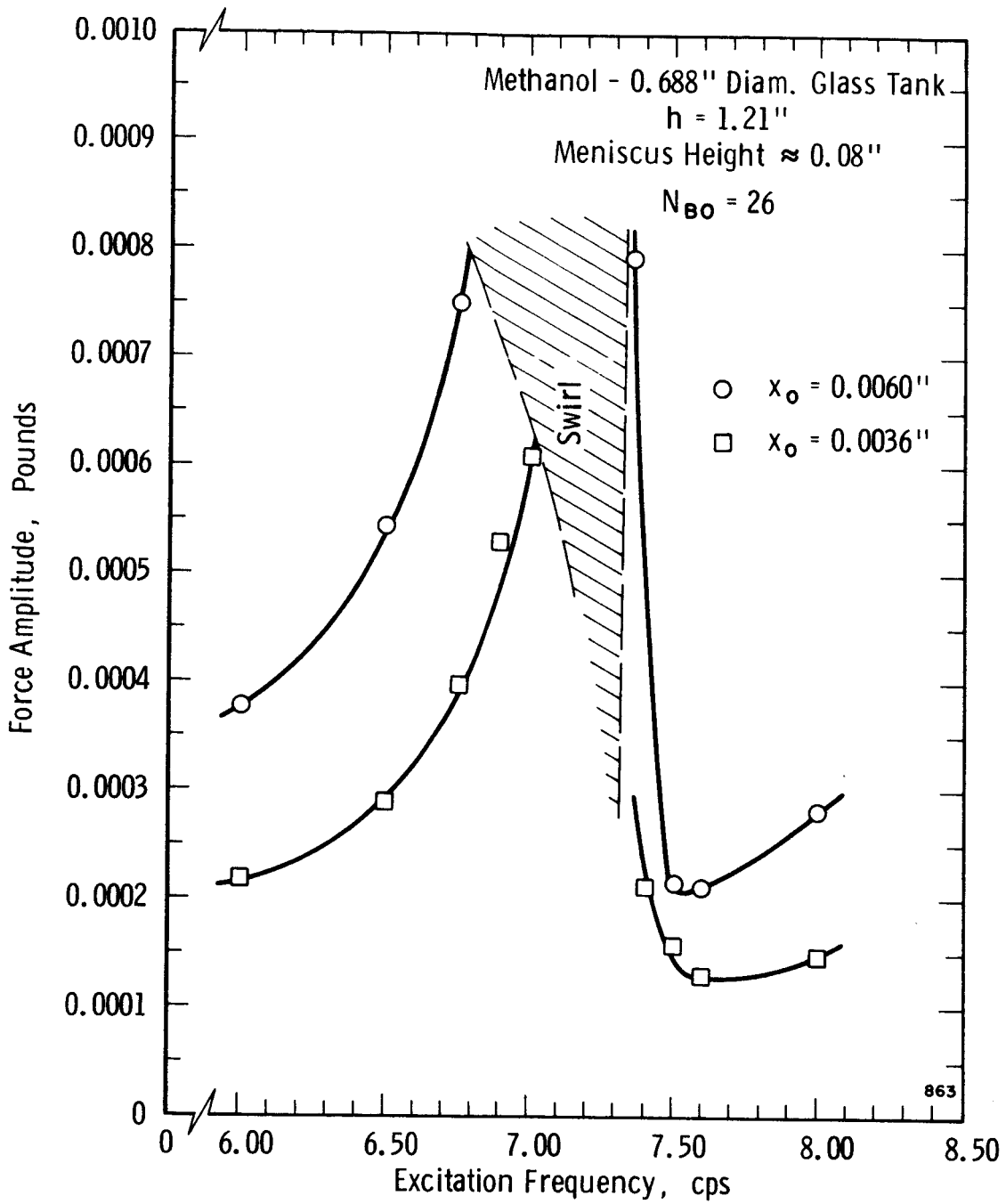
Figure 15. Response Curve For Methanol, Bond Number = 26
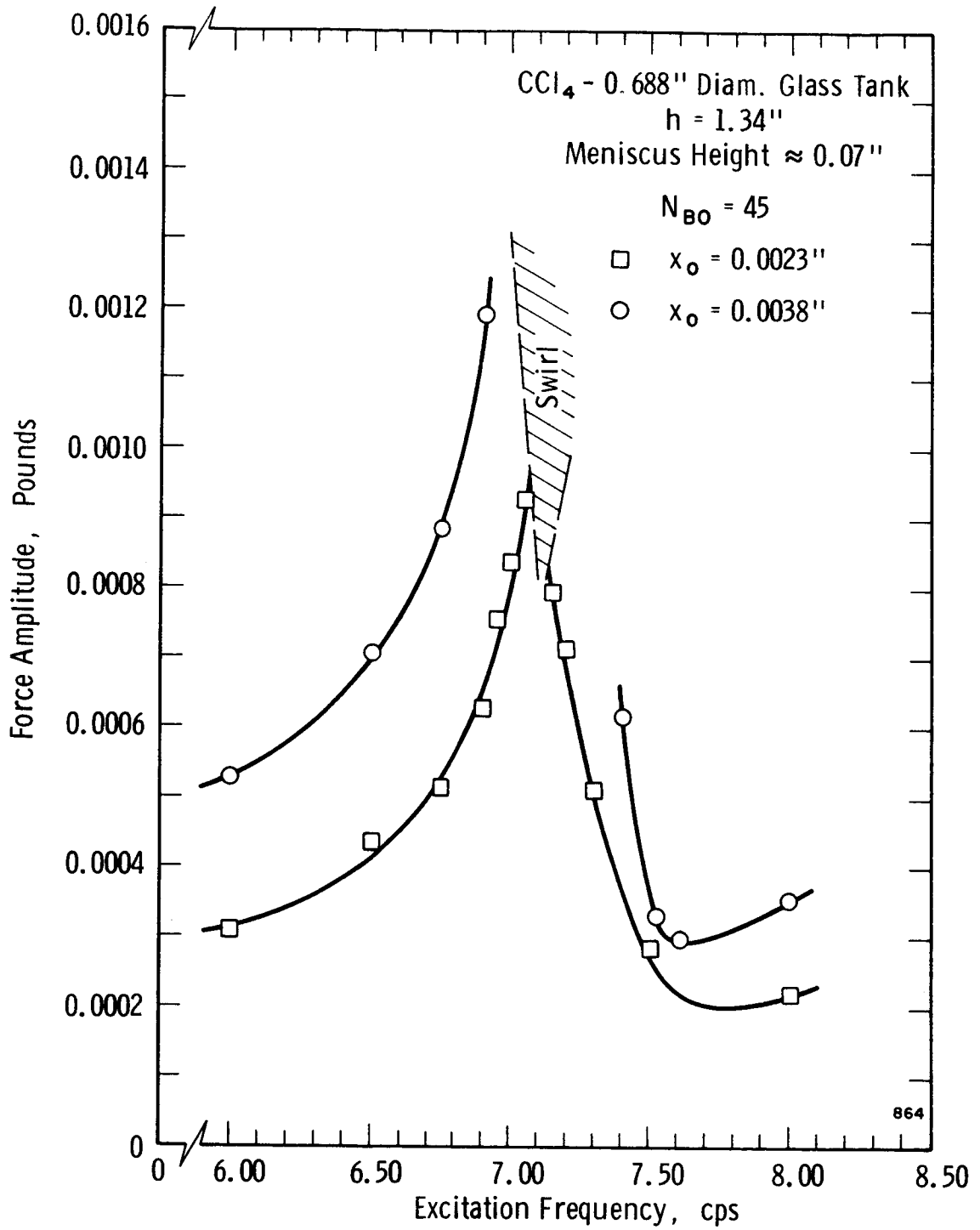
Figure 16.   Response Curve For Carbon Tetrachloride, Bond Number = 45
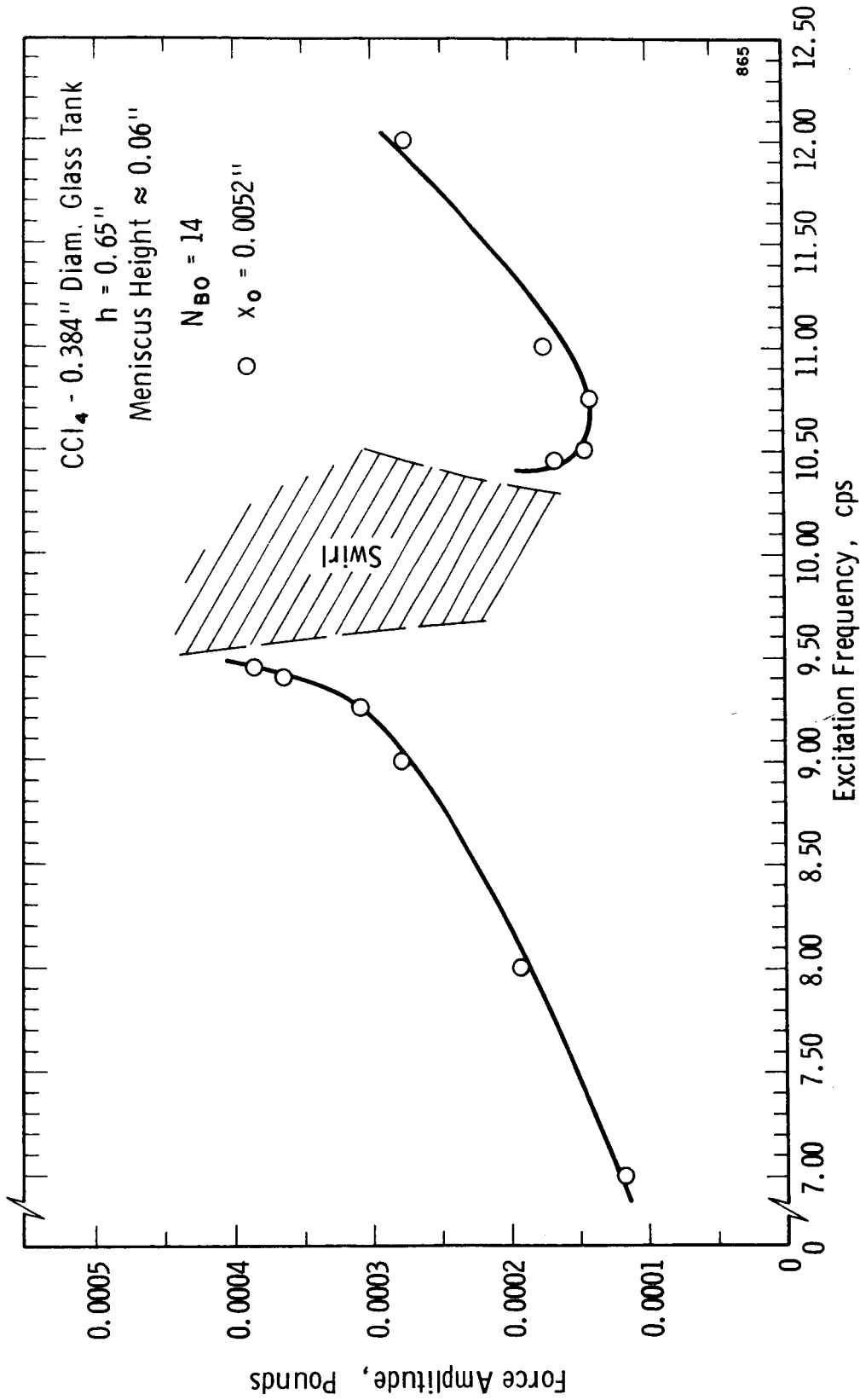
Figure 17.   Response Curve For Carbon Tetrachloride, Bond Number = 14
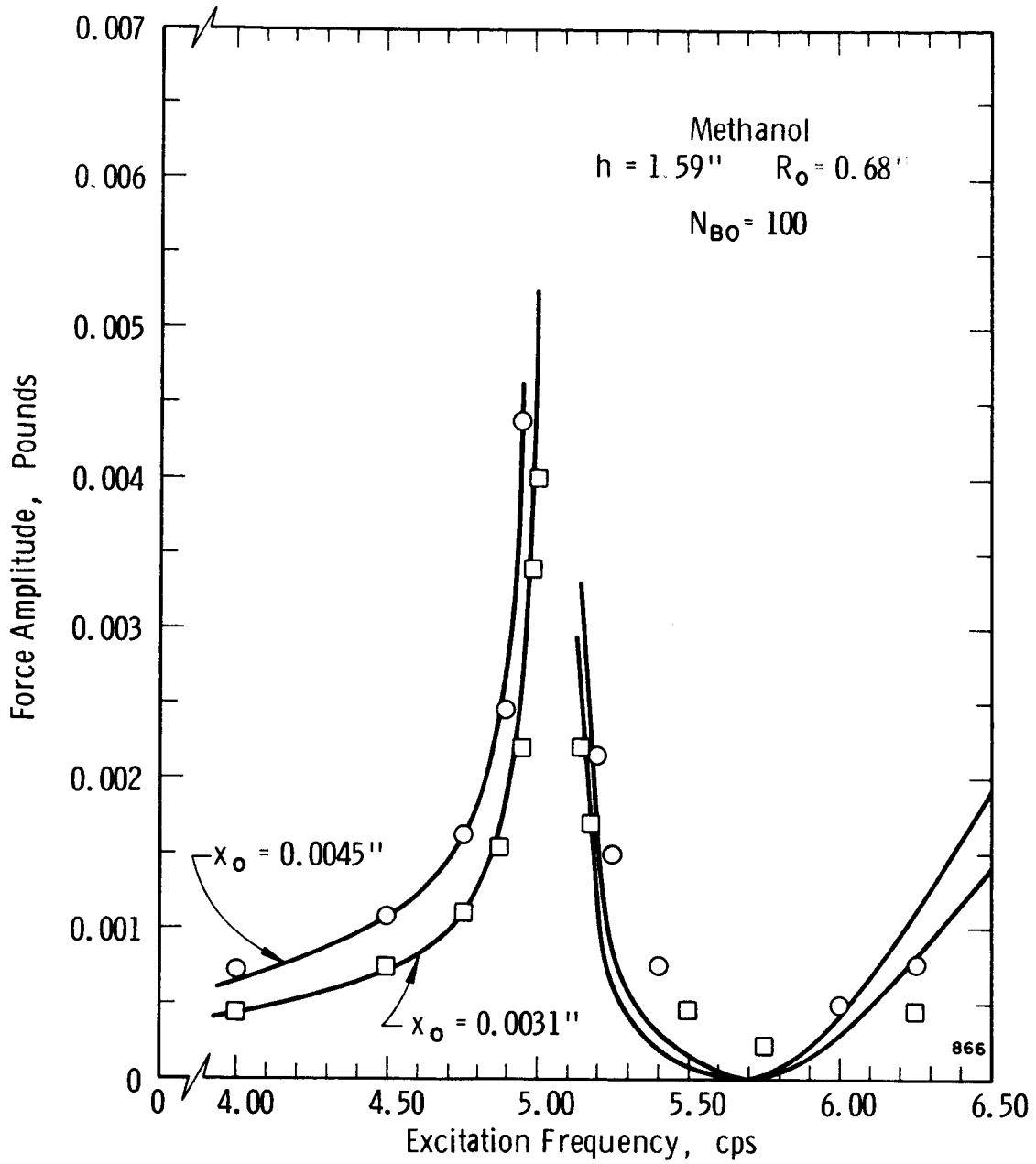
Figure 18. Comparison Of Theory And Experiment, $N_{BO} = 100$
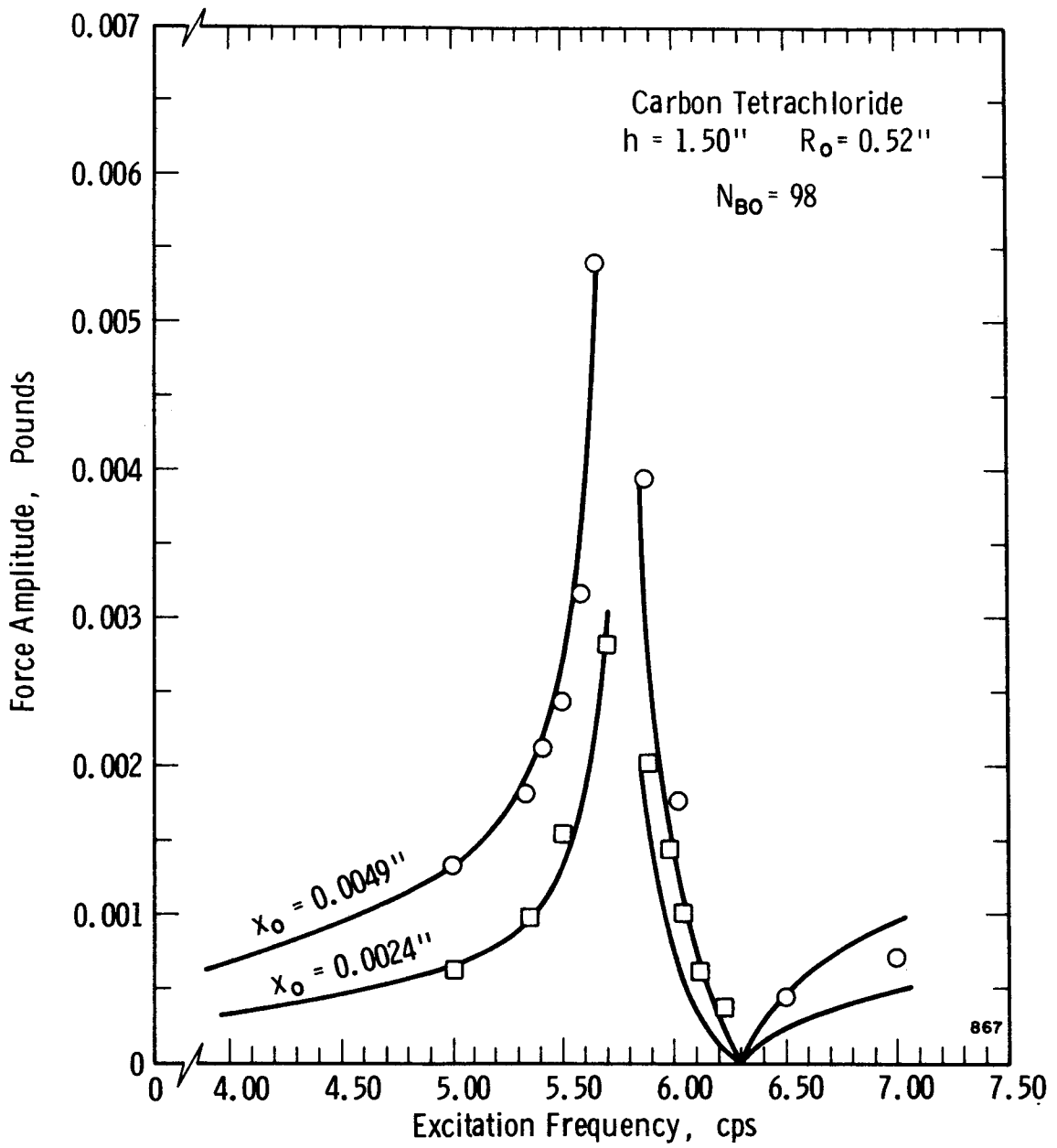
Figure 19. Comparison Of Theory And Experiment, $N_{BO} = 98$
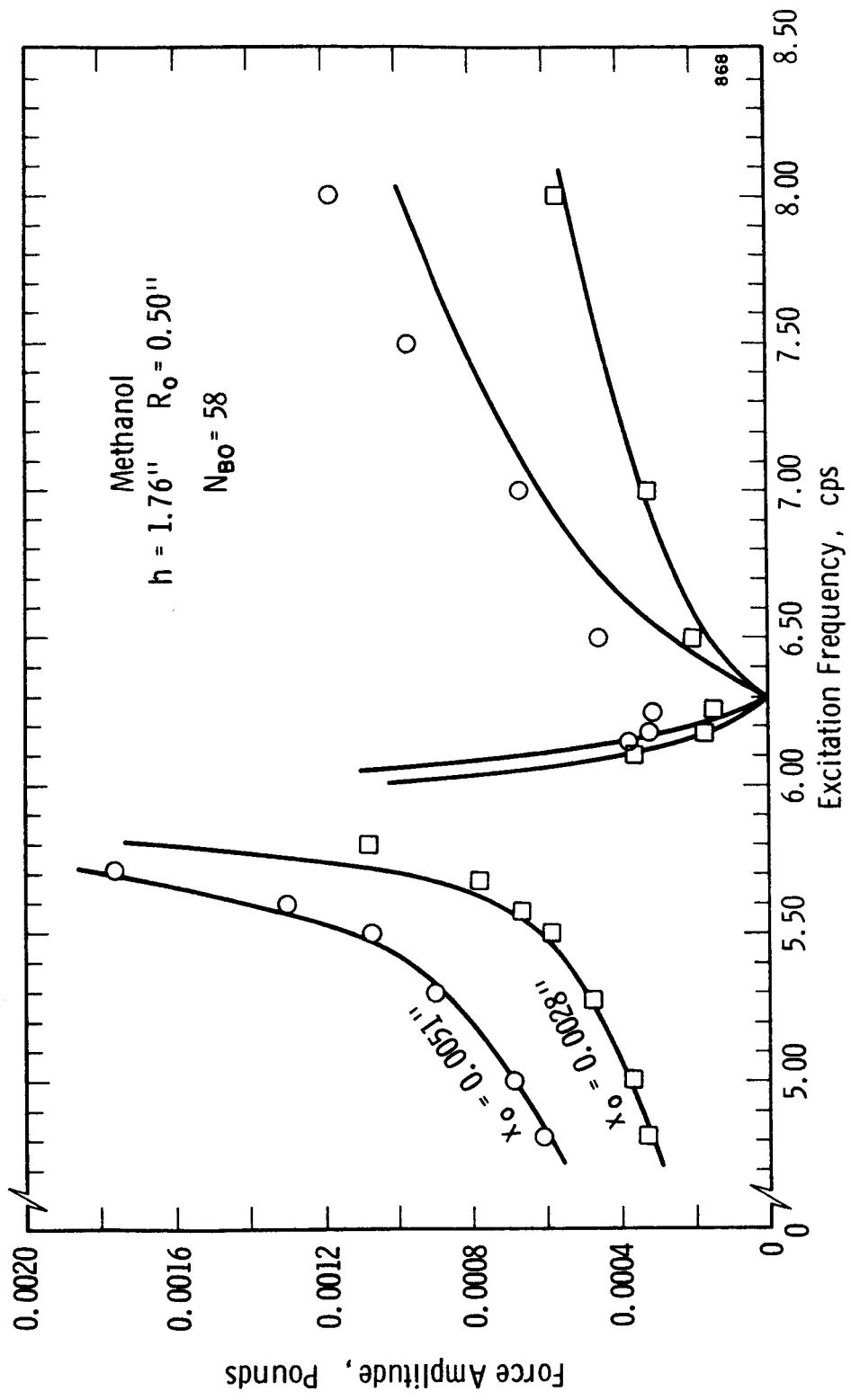
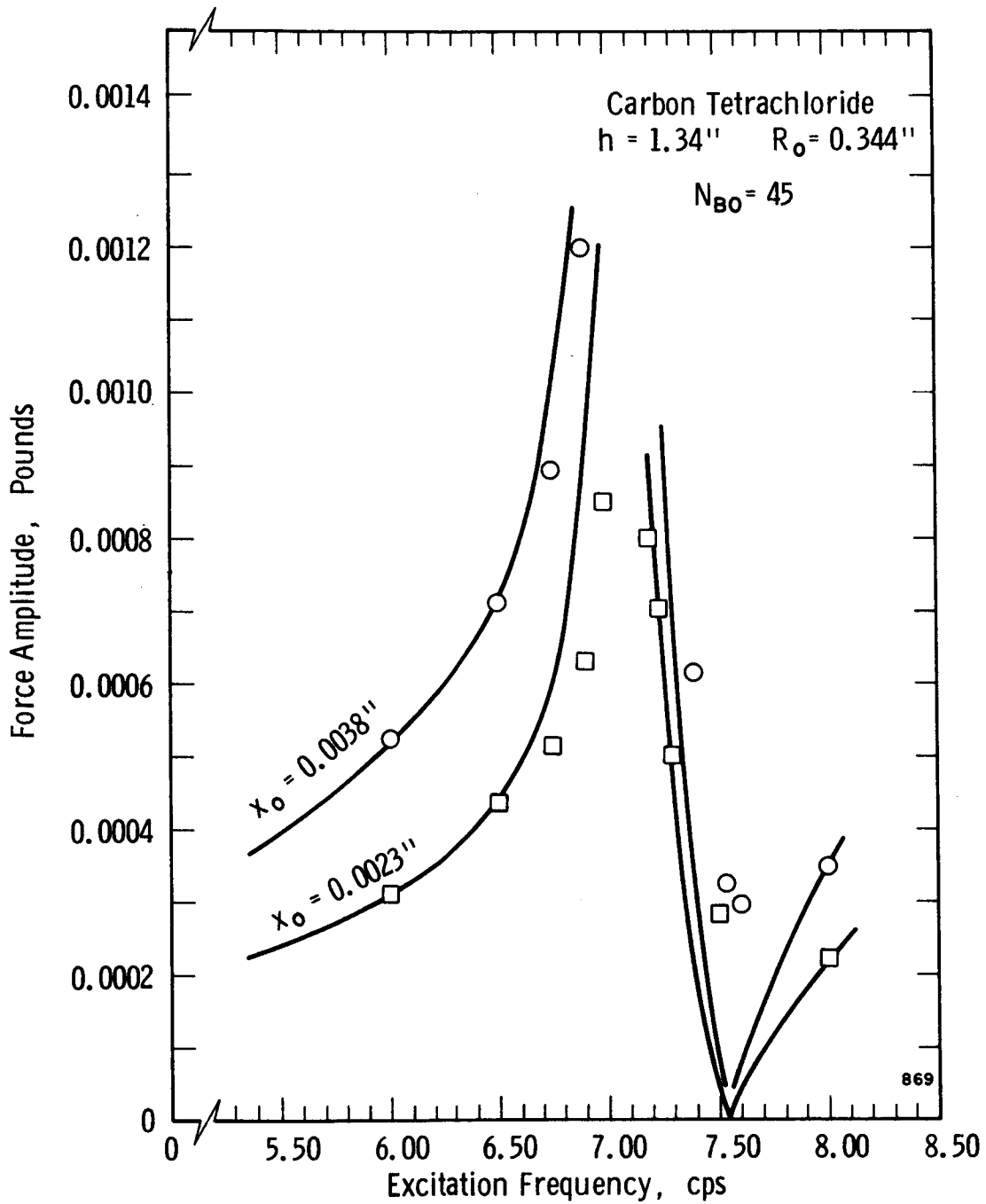Figure 20. Comparison Of Theory And Experiment, $N_{BO} = 58$

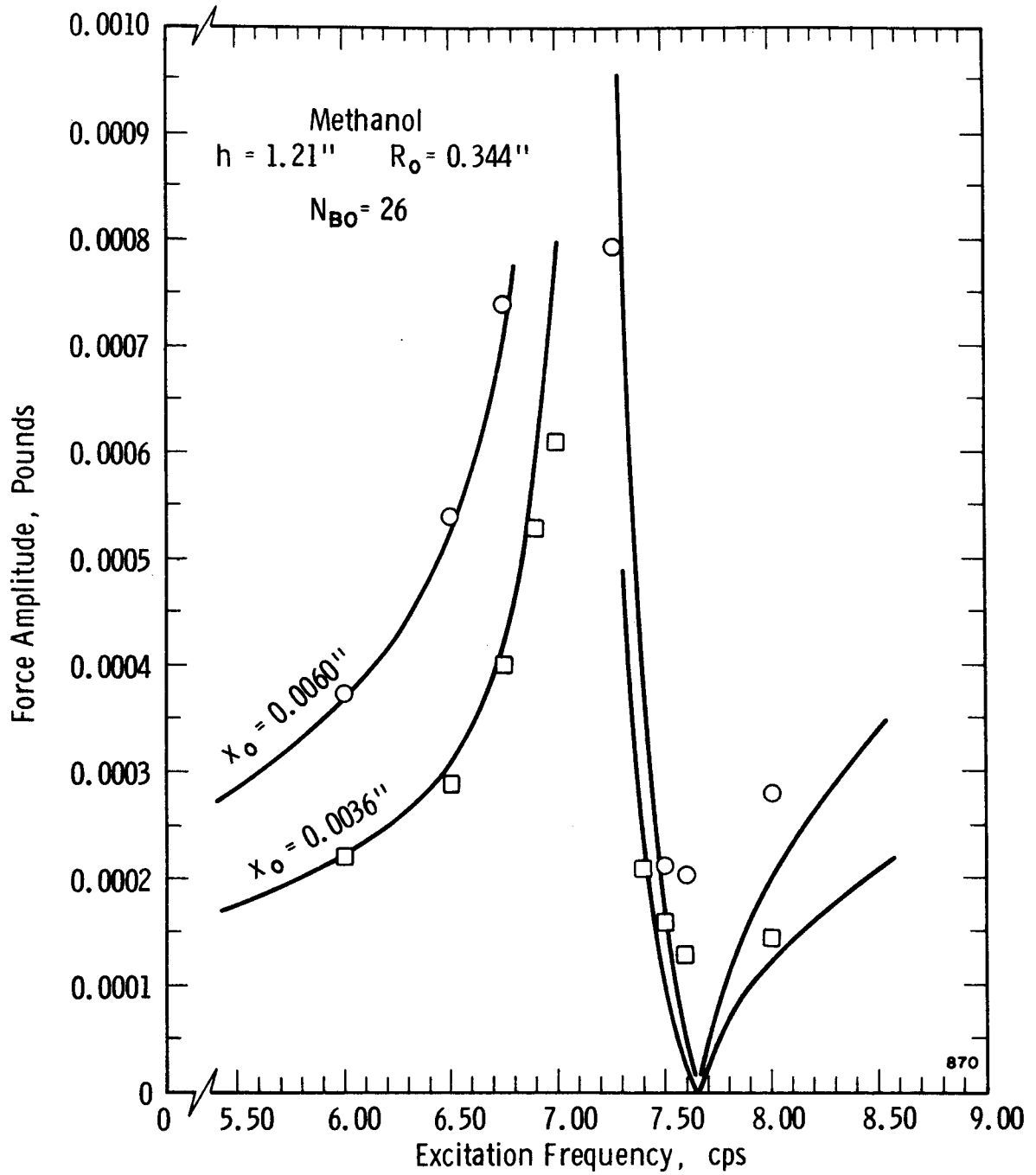Figure 21. Comparison Of Theory And Experiment, $N_{BO} = 45$
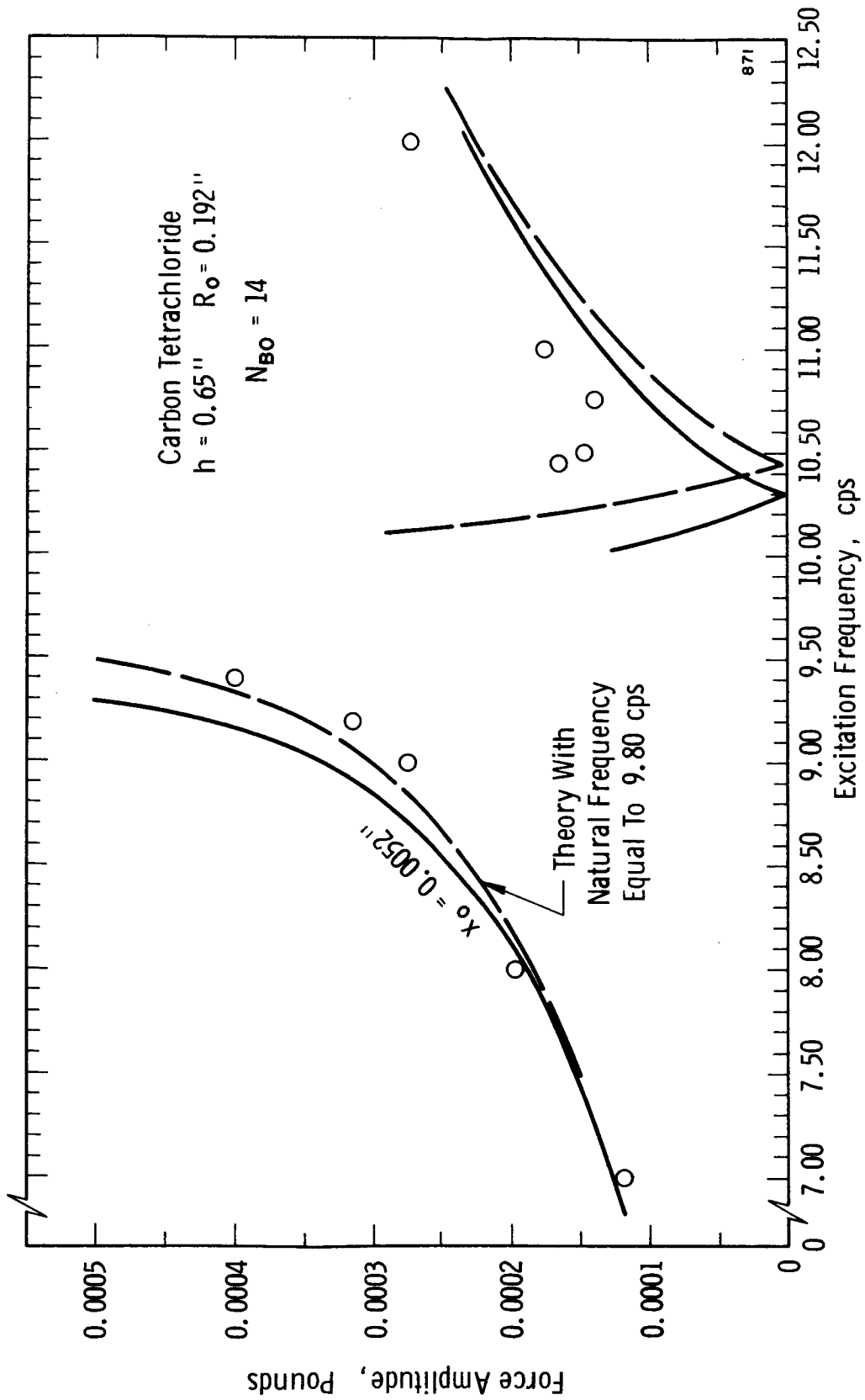
Figure 22. Comparison Of Theory And Experiment, $N_{BO} = 26$

Figure 23. Comparison Of Theory And Experiment, $N_{BO} = 14$